

Journal Pre-proofs

Hydrophobic deep eutectic solvent (HDES) as oil phase in lipid-based drug formulations

Shaida Panbachi, Josef Beranek, Martin Kuentz

PII: S0378-5173(24)00652-5
DOI: <https://doi.org/10.1016/j.ijpharm.2024.124418>
Reference: IJP 124418

To appear in: *International Journal of Pharmaceutics*

Received Date: 25 April 2024
Revised Date: 28 June 2024
Accepted Date: 1 July 2024

Please cite this article as: S. Panbachi, J. Beranek, M. Kuentz, Hydrophobic deep eutectic solvent (HDES) as oil phase in lipid-based drug formulations, *International Journal of Pharmaceutics* (2024), doi: <https://doi.org/10.1016/j.ijpharm.2024.124418>

This is a PDF file of an article that has undergone enhancements after acceptance, such as the addition of a cover page and metadata, and formatting for readability, but it is not yet the definitive version of record. This version will undergo additional copyediting, typesetting and review before it is published in its final form, but we are providing this version to give early visibility of the article. Please note that, during the production process, errors may be discovered which could affect the content, and all legal disclaimers that apply to the journal pertain.

© 2024 The Author(s). Published by Elsevier B.V.



1 **Hydrophobic deep eutectic solvent (HDES) as oil phase in lipid-**
2 **based drug formulations**

3

4 *Shaida Panbachi^{a-c}, Josef Beranek^a, Martin Kuentz^{c*}*

5 ^a *Zentiva, k.s., U Kabelovny 130, 102 00 Praha 10, Czech Republic*

6 ^b *University of Basel, Department of Pharmaceutical Sciences, Klingelbergstrasse 50,*
7 *4056 Basel, Switzerland*

8 ^c *University of Applied Sciences and Arts Northwest. Switzerland, School of Life Sciences,*
9 *Institute of Pharma Technology, Hofackerstr. 30, CH- 4132 Muttenz, Switzerland*

10 * Correspondence to: Prof. Dr. Martin Kuentz (Telephone: +41-612285642; E-mail
11 address: martin.kuentz@fhnw.ch

12

13 **Abstract**

14

15 There is increasing pharmaceutical interest in deep eutectic solvents not only as a
16 green alternative to organic solvents in drug manufacturing, but also as liquid formulation
17 for drug delivery. The present work introduces a hydrophobic deep eutectic solvent
18 (HDES) to the field of lipid-based formulations (LBF). Phase behavior of a mixture with
19 2:1 molar ratio of decanoic- to dodecanoic acid was studied experimentally and described
20 by thermodynamic modelling. Venetoclax was selected as a hydrophobic model drug and
21 studied by atomistic molecular dynamics simulations of the mixtures. As a result, valuable
22 molecular insights were gained into the interaction networks between the different
23 components. Moreover, experimentally the HDES showed greatly enhanced drug
24 solubilization compared to conventional glyceride-based vehicles, but aqueous
25 dispersion behavior was limited. Hence surfactants were studied for their ability to
26 improve aqueous dispersion and addition of Tween 80 resulted in lowest droplet sizes
27 and high in vitro drug release. In conclusion, the combination of HDES with surfactant(s)
28 provides a novel LBF with high pharmaceutical potential. However, the components must
29 be finely balanced to keep the integrity of the solubilizing HDES, while enabling sufficient
30 dispersion and drug release.

31

32 **Key words:** Deep eutectic solvent(s), eutectic(s), poorly soluble drug(s), lipid-based
33 formulation(s), novel pharmaceutical(s), advanced formulation(s)

34

35 1 Introduction

36 Deep eutectic solvents (DES) have been reported as an attractive solubilization
37 technology with potentially a several thousand-fold increase in solubility relative to water
38 (Faggian et al., 2016; Fourmentin et al., 2021; Jeliński et al., 2019; Li & Lee, 2016; Sut et
39 al., 2017). Several studies have also shown that this holds true when dissolving
40 pharmaceutically active ingredients (APIs) that are otherwise poorly soluble (Faggian et
41 al., 2016; Fourmentin et al., 2021; Huber et al., 2022; Li & Lee, 2016; Morrison et al.,
42 2009; Palmelund et al., 2019). Notable examples include aprepitant and indomethacin,
43 where solubility in the respective DES yielded 6.78 ± 0.03 mg/g (1057-fold higher than
44 the aqueous solubility) for the former and 175.6 ± 3.428 mg/mL ($\approx 159'000$ - fold higher
45 than the aqueous solubility) for the latter API (Palmelund, Eriksen, et al., 2021; Panbachi
46 et al., 2023). DES are generally considered as a worthwhile alternative to organic solvents
47 and ionic liquids due to potentially better oral tolerability (Benvenuti et al., 2019; Dai et
48 al., 2013; Fourmentin et al., 2021; Hansen et al., 2021; Ramón & Guillena, 2019).
49 Traditionally, DES have mainly been studied and utilized in the field of green chemistry
50 and chemical engineering, mostly by relying on the strong solubilization effects of the
51 liquids applied (Fourmentin et al., 2021; Hansen et al., 2021; Martins et al., 2019; Morrison
52 et al., 2009; Ramón & Guillena, 2019). However, these mixtures also present great
53 underexplored potential in the field of pharmaceuticals where such mixtures could either
54 hold for an intermediate bulk solution or even the final drug product (Abranches &
55 Coutinho, 2023; Oyoun et al., 2023; Palmelund, Eriksen, et al., 2021; Palmelund et al.,
56 2019; Panbachi et al., 2023).

57 A deep eutectic solvent (DES) is described as a mixture of two or more hydrogen bond
58 acceptors (HBAs) and donors (HBDs), interacting at a specific molar ratio, resulting in a
59 eutectic point that is lower than that of the hypothetical eutectic point at ideal conditions
60 (Abranches & Coutinho, 2023; Fourmentin et al., 2021; Hansen et al., 2021; Martins et
61 al., 2019). This is the distinct characteristic of DES (Martins et al., 2019). Furthermore,
62 these liquids have been described as thermodynamically stable in their liquid state and
63 can be liquid at room- and/or operating temperatures depending on their eutectic point
64 (Abdelquader et al., 2023; Ghaedi et al., 2018). These beneficial properties make DES a
65 viable option in the development of a solubility-improving formulation for poorly water-
66 soluble APIs (Abdelquader et al., 2023; Palmelund, Eriksen, et al., 2021; Panbachi et al.,
67 2023).

68 As mentioned above, the clear deviation in thermodynamic behavior of DES from the
69 ideal melting point depression, distinguishes it from other eutectic solutions (Martins et
70 al., 2019). This can be deemed a 'strict' definition of a DES, because previous literature
71 often used the term broadly from a practical application point of view without providing
72 phase diagrams. Therefore, several DES experts recently encouraged researchers to
73 supply newly described DES with phase diagrams to better distinguish eutectic mixtures
74 from true DES (Abranches & Coutinho, 2023; Martins et al., 2019; Palmelund, Rantanen,
75 et al., 2021). Accordingly, the current work provides such phase diagrams using the
76 Schröder van Laar (SvL) equation, thereby describing a solid-liquid line for 'ideal' mixture
77 conditions (i.e., using an activity coefficient of 1), which is compared to an experimental
78 phase diagram (Palmelund et al., 2020; Wolbert et al., 2019). Moreover, universal

79 **quasichemical functional** group activity coefficients (UNIFAC) were considered as a
80 predictive thermodynamic model to compare with experimental data and to identify
81 possible model improvements compared to the ideal SvL equation. This approach has
82 been pioneered in the field of therapeutic DESs (THEDESSs) by Wolbert et al., 2019. As
83 a result, the UNIFAC model proved to be adequate to describe the selected model
84 systems. More work should be done based on this thermodynamic approach to study not
85 only THEDESSs, where the drug is a constituting deep eutectic component, but also DES
86 as a solvent mixture for drugs.

87 DES are divided into 5 categories of mixtures (I-V) depending on the chemistry of the
88 components employed (Abranches et al., 2019; Fourmentin et al., 2021). Type III DESs
89 are made of organic HBD and HBAs, which have been described as the most suitable
90 candidates for pharmaceutical development due to their comparatively better oral
91 tolerability (Abdelquader et al., 2023; Abranches & Coutinho, 2023; Fourmentin et al.,
92 2021; Oyoun et al., 2023; Palmelund et al., 2019). Within this category, further
93 subcategories can be described based on the properties of the constituent components,
94 which ultimately determine the physicochemical properties of the final DES formulation.
95 For example, natural deep eutectics, a known subcategory of class III deep eutectics, are
96 referred to as “natural” due to the use of components with natural origins; these include
97 primary metabolites such as organic acids, amino acids, sugars, polyols, and choline
98 derivatives, which show low toxicity (Fourmentin et al., 2021). These “natural” DES or
99 NADES have been deemed viable candidates for drug product development and
100 environmental applications (Dai et al., 2013; Faggian et al., 2016; Fourmentin et al., 2021;
101 Huber et al., 2022; Jeliński et al., 2019; Liu et al., 2018; Sut et al., 2017).

102 Another example of components that govern final DES formulation properties are
103 hydrophobic deep eutectic solvents (HDESs). These are another subcategory of class III
104 DES comprised of hydrophobic components (Florindo et al., 2018; Fourmentin et al.,
105 2021; Ramón & Guillena, 2019; Van Osch et al., 2020; Zainal-Abidin et al., 2021). They
106 have been described in the literature and studied for their extraction capabilities in
107 chemical sustainability and engineering (Florindo et al., 2018; Van Osch et al., 2020;
108 Zainal-Abidin et al., 2021). However, to our knowledge, HDES have not been studied for
109 pharmaceutical applications (Van Osch et al., 2020). Using HDES either directly or with
110 further added excipient(s), could pave the way for novel pharmaceutical applications.

111 In this study, an HDES is investigated as an alternative to traditionally used oils in lipid-
112 based formulations (LBFs) to enable a viable formulation of venetoclax. The latter drug is
113 known to be a BCS (biopharmaceutical classification system) class IV API (Emami
114 Riedmaier et al., 2018; Shah & Amidon, 2014) that does not meet the criteria of ‘Lipinski’s
115 rule of 5’ (DeGoey & Cox, 2021; Hartung et al., 2023) and the compound shows a high
116 lipophilicity ($\log P > 4$) (Koehl et al., 2019, 2021). It is a hypothesis of the current work that
117 HDES could be a useful formulation approach for overcoming the biopharmaceutical drug
118 delivery issues of such APIs. The particular HDES used in this study is made of a 2:1
119 molar ratio of decanoic acid (DeA) to dodecanoic acid (DoA), which has previously been
120 described in two articles on extraction techniques and environmental chemistry
121 (Dwamena, 2019; L. Wang & Meng, 2010). The present study targeted novel
122 pharmaceutical applications by first studying the phase behavior, both experimentally and

123 theoretically, using SvL and UNIFAC modelling. It also aimed to achieve a molecular
124 understanding by using full atomistic molecular dynamics (MD) simulations of the pure
125 DES as well as of the DES mixtures containing venetoclax. A further study aim was to
126 explore the aqueous dispersion behavior of the selected HDES by considering surfactant
127 addition (Tween 80) for development of an innovative lipid-based formulation (LBF).

128 **2 Materials and methods**

129 Venetoclax was purchased from Laurus Labs Ltd. (Telangana, India). The DES
130 components decanoic acid (DeA) and dodecanoic acid (DoA), the surfactants Cremophor
131 EL, DL- α -tocopherol methoxypolyethylene glycol succinate (TPGS) and Poloxamer 188,
132 along with buffer components, HPLC-grade acetonitrile ($\geq 99.9\%$), ammonium phosphate
133 monobasic and phosphoric acid solution for pH adjustments, were all purchased from
134 Sigma-Aldrich (Sigma-Aldrich, Steinheim, Germany). Medium chain triglyceride Miglyol®
135 812 N was kindly provided as a free sample from IOI Oleochemicals (IOI Oleo GmbH,
136 Hamburg, Germany). Gelucire 48/16, Labrasol ALF, Labrafac lipophile WL 1349, and
137 Labrafil M2125 CS were also provided as free samples from Gattefossé (Saint-priest,
138 France), and the Soluplus® was purchased from BASF (BASF SE, Ludwigshafen,
139 Germany). Tween 80 (Ph.Eur. grade) was purchased from Carl Roth GmbH & Co. KG
140 (Karlsruhe, Germany) and food-grade sesame oil was purchased from Momentum Foods
141 Pty Ltd. (Melbourne, Australia).

142 **2.1 Preparation and physical characterization of HDES**

143 The hydrophobic deep eutectic solvent (HDES) consisted of decanoic acid (DeA)
144 and dodecanoic acid (DoA) at the molar ratio of 2:1. The mixture was placed on a heating
145 plate set to 70°C, and stirred for 2 h (Dwamena, 2019). The maximum batch sizes
146 prepared were 60 g and prepared HDESs were stored in an oven at a constant
147 temperature of 25°C.

148 The dynamic viscosity of the prepared liquid was measured in triplicate at ambient
149 room temperature using the Turning Fork Vibro Viscometer SV-10A (A&D Company Ltd.,
150 Tokyo, Japan) at 30 Hz vibration. Prior to measurement, the instrument was adjusted
151 using a one-point calibration method with water as the standard reference. Density was
152 measured in triplicate at ambient temperature using oscillation that was induced
153 electromagnetically in the glass U-tube of the DA-100M densitometer (Mettler Toledo,
154 Greifensee, Germany). The measurement was performed in triplicate on 1 mL samples
155 injected into the tube.

156 Water content was measured in triplicate by a volumetric Karl-Fischer titration (KFT)
157 instrument (Titrand 841 KFT, Metrohm Schweiz AG, Herisau, Switzerland). The titration
158 factor was determined by the titration of 30 μ L purified water using a 1 mL graduated
159 calibrated microliter syringe with cemented needle (Hamilton Storage GmbH, Domat,
160 Switzerland) and Titrant 5 as the titrant. The prepared HDES samples were diluted with
161 methanol to give a solution with a concentration of 1 g/mL of water-containing-HDES in
162 solvent. A 1 mL plastic syringe (Injekt®-F Luer Solo syringe, B. Braun Medical AG,
163 Sempach, Switzerland) fitted with a needle (100 Sterican®, 20 G x 1 ½, B. Braun Medical

164 AG, Sempach, Switzerland) was then used to inject 1 mL of the solution in the titration
165 medium (Aqustar®, Merck KGaA, Taufkirchen, Germany). The water content and titration
166 graph were then obtained by the Tiamo software version 2.4 (Metrohm, Herisau,
167 Switzerland).

168 **2.2 In-silico prediction of HDES phase diagram**

169 The melting point of the individual molar ratios of the HDES was calculated using
170 the Schröder van Laar equation (Prigogine & Defay, 1954; Umerska et al., 2020). This
171 equation is derived from the Van't Hoff equation (Deiters, 2012) by assuming an ideal
172 thermodynamic binary system where the activity coefficient (γ_i) is equivalent to one
173 (Deiters, 2012; Prigogine & Defay, 1954; Wolbert et al., 2019). The following equation 1
174 describes the liquid-solid phase equilibrium, which corresponds to the Schröder van Laar
175 equation in the event that the activity coefficient γ_i is unity (Chakraborty et al., 2021;
176 Prigogine & Defay, 1954; Umerska et al., 2020; Wolbert et al., 2019):

$$177 \quad \ln(\chi_i \cdot \gamma_i) = -\frac{\Delta H_i}{R} \left(\frac{1}{T} - \frac{1}{T_{mi}} \right) \text{ (Equation 1)}$$

178 The equation includes temperature T , melting point T_{mi} of a component i based on
179 the molar fraction (χ_i), and the fusion enthalpy (ΔH_i) of component i (Prigogine & Defay,
180 1954). This equation is applied to both components in selected molar fractions from 0-1,
181 increasing with consecutive 0.005 increments resulting in two different solid-liquid lines
182 (SL-line) (Prigogine & Defay, 1954; Umerska et al., 2020; Wolbert et al., 2019). The
183 trendlines of the two SL-lines are combined on a 'two-way' x-axis depicting the
184 incremental increase in the molar fraction of one component from left to right, and the
185 other component from right to left, where the intersection of the two lines provides the
186 eutectic point on the phase diagram (Wolbert et al., 2019). When predicting the
187 thermodynamic system's behavior in 'ideal conditions', the activity coefficient (γ_i) in
188 equation 1 is unity (SvL), while activity coefficients were also calculated according to the
189 UNIFAC approach as described below.

190 **2.2.1 Prediction of activity coefficients using UNIFAC**

191 The UNIFAC model is a universal **quasichemical functional** group contribution model
192 to predict the activity coefficients of nonelectrolyte liquid mixtures (Fredenslund et al.,
193 1975). The model assumes short-range order and long-range disorder and that the
194 thermodynamic properties of a mixture are largely determined by the first neighbor's
195 interactions (Abusleme & Vera, 1985; Fredenslund et al., 1975; Skjold-Jorgensen et al.,
196 1979). UNIFAC is based on group contributions in that a molecule is split into different
197 structural/functional groups where every group has specific group parameters and
198 interaction parameters with other groups. Each molecule can be assembled based on
199 these building blocks within the model to enable calculation of diverse chemicals. Since
200 no experimental data is needed, UNIFAC is a fully predictive method to estimate activity
201 coefficients (Abusleme & Vera, 1985; Fredenslund et al., 1975; Skjold-Jorgensen et al.,
202 1979; Wolbert et al., 2019). Molecular Modeling Pro Flavor Plus (version 9.1.20) was used
203 as an extension tool on the ChemElectrica gateway software (version 4.0.5) to calculate

204 the respective UNIFAC activity coefficients. The values were estimated for standard
205 conditions at 298.15 K, thereby avoiding the temperature dependence that was previously
206 evaluated to have only minor effects (i.e., on the third decimal) on estimated activity
207 coefficients.

208 **2.3 Depiction of phase diagram using experimentally obtained melting points**

209 The HDES experimental phase diagram was determined by depicting the mixture's
210 solid-liquid line from melting points of different molar fractions of the two components
211 (Wolbert et al., 2019). The melting point was measured using the differential scanning
212 calorimetry (DSC) Pyris 1 (Perkin Elmer Inc., Norwalk, USA) connected to a cooling
213 system (Perkin Elmer Inc., Norwalk, USA) programmed to perform a ramp cycle from -
214 10°C to +50°C, with a nitrogen purge of 50 mL/min, at a heating rate of 1°C/min. The
215 molar fractions of the physical mixtures studied increased incrementally from 0:1 to 1:0
216 of DeA:DoA. Two additional molar fractions corresponding to those derived from the
217 predicted eutectic points (section 2.2), were also investigated.

218 To avoid spontaneous formation of the HDES during preparation, the physical
219 mixtures were prepared using refrigerated components (-21°C). The mixtures were briefly
220 ground using a pestle and mortar in a cooled environment using cooling packs in a
221 Styrofoam box, after which the samples were immediately refrigerated again (5 ± 3 °C).
222 5-8 mg of the prepared samples were transferred into standard aluminum pans (Perkin
223 Elmer Inc., Norwalk, USA), and sealed with standard aluminum covers (Perkin Elmer Inc.,
224 Norwalk, USA). The DSC sample chamber was cooled to -10°C prior to the measurement
225 to ensure that the DSC sample chamber temperature would not result in spontaneous
226 melting of the components. The thermograms obtained were analyzed using the Pyris
227 software (version 11.1.0.0488). The endothermic peaks on the thermograms (determined
228 in triplicate) were directed upwards and the onset point of the most prominent peak was
229 selected as the melting point of the respective mixture to construct the solid-liquid line of
230 the mixture (Umerska et al., 2020; Wolbert et al., 2019).

231 **2.4 Molecular dynamics simulations of HDES**

232 The molecular dynamics (MD) simulations were performed using the YASARA
233 software version 20.12.24 (YASARA Biosciences GmbH, Vienna, Austria) (Krieger &
234 Vriend, 2014). The simulations were based on pure HDES (DeA:DoA, 1:2) and HDES
235 with 5% w/w venetoclax (each with n=4 simulation runs). To fit a cuboid simulation box
236 with the dimensions of 65x65x65 Å, a number of 496 molecules of DeA and 248
237 molecules of DoA was selected to represent the pure HDES. The 5% w/w venetoclax
238 loaded system was analogous with eight molecules of API in the simulation box. An
239 AMBER-type all atom force field (GAFF2) (Wang et al., 2004) was selected, for which
240 atom charges were based on a semi-empirical quantum chemical estimation (AM1BCC)
241 (Jakalian et al., 2002); long-range interactions were estimated using an 8 Å cut-off value
242 for the mesh Ewald method as implemented in YASARA. To bring about initial random
243 molecular orientations, an initial closed wall (i.e., NVT) cycle was run at 600 K for 5 ns,
244 whereby the motion equations were integrated with 2x 1 fs steps. The main simulation
245 cycle was then run using an NPT ensemble for a total time of 20 ns (2x 1 fs steps), using

246 the set temperature of 298 K under periodic boundary conditions. The temperature control
247 was attained through rescaled atom velocities using a weakly coupling thermostat, to
248 keep the macroscopic temperature at the required value of 298 K. To avoid artifacts
249 arising from the classically used Berendsen thermostat, a scaling factor was calculated
250 according to the Berendsen formula from the time average temperature, thereby avoiding
251 use of the strongly fluctuating instantaneous microscopic temperature for velocity
252 rescaling at the individual simulation steps (Zhou & Liu, 2022). Finally, the molecular
253 interactions from eight sampling points within 200 ps following the second cycle were
254 analyzed for all simulation runs (each with $n=4$).

255 2.5 Determination of apparent solubility values

256 An excess of API was added to the liquid so that a slight residue of particles could
257 be seen suspended at the end of the stirring times. This was mainly due to a paste-like
258 phase separation seen at higher amounts of excess API, creating technical difficulty
259 separating the liquid phase for analysis. Accordingly, a maximum concentration of about
260 130 mg/mL was used to prepare the samples for which the solubility was studied (using
261 subsequent centrifugation and filtration as described below).

262 A sample volume of 3 mL with the excess venetoclax was transferred to a 20 mL
263 clear headspace vial of 22.5 x 75 mm (Supelco, Sigma-Aldrich, Steinheim, Germany),
264 sealed using 20 mm aluminum pressure release seals (with PTFE/rubber liner, Supelco,
265 Sigma-Aldrich, Steinheim, Germany) and stirred for 24 h at 350 rpm using a magnetic
266 stirring bar (PTFE-coated, cylindrical with pivot ring, L 12 mm, bar diameter 4.5 mm,
267 BRAND®, Sigma-Aldrich, Steinheim, Germany) on a stirring plate (IKA® RCT basic,
268 Staufen, Germany) at ambient conditions. 2 mL of the sample volume was transferred to
269 a 2 mL safe-lock Eppendorf® tube (Eppendorf AG, Hamburg, Germany) and centrifuged
270 at 14000 rpm for 30 min, in a centrifuge (MPW-65R, MPW Med. Instruments, Warszawa,
271 Poland) with a maximum relative centrifugal force of 20160 x g. A 100 μ L sample was
272 then extracted from the supernatant obtained using a positive displacement pipette
273 (Repetman HandyStep®, Gilson, Villiers-Le-Bel, France) with the respective pipette tips
274 (PD-Tips II, Fischer Scientific, Wertheim, Germany) and diluted with a factor of 1:1000
275 (v/v) in the mobile phase (described in section 2.5.1 below). In case of the long- and short
276 chain triglyceride (sesame oil and Miglyol 812N) samples, a solvent made of the mobile
277 phase constituents adjusted to 85:15 (v/v) was used in the first round of dilution (with a
278 factor of 1:100) and further diluted to a total factor of 1:1000 using the 70:30 v/v mobile
279 phase. The FeSSIF-V2 (Marques, 2004) (Biorelevant, London, UK) biorelevant media
280 described in section 2.9 was only diluted to 1:100 using the mobile phase. All diluted
281 samples were stirred overnight, after which they were filtered using a 0.45 μ m filter (ProFill
282 PA, 0.45 μ m, Fisher Scientific, Wertheim, Germany) mounted to 3 mL syringes (Injekt®-
283 F Luer Solo syringe, B. Braun Medical AG, Melsungen, Germany) and filled into amber
284 crimp-top 2 mL HPLC vials (Agilent Technologies Co. Ltd., Beijing, China), sealed with
285 caps (silver, PTFE/silicone septa for 2 mL vials, Agilent Technologies Co. Ltd., Beijing,
286 China) and measured using the method described below (section 2.5.1). The study was
287 performed in three separate sample batches, to make up a triplicate analysis.

288 **2.5.1 Quantification of dissolved API using HPLC**

289 High performance liquid chromatography (HPLC) was used to determine the
290 venetoclax content in the samples. The instrument employed was an Agilent 1100 Series
291 Capillary LC System (Agilent Technologies AG, Basel, Switzerland). The mobile phase
292 consisted of a volumetric ratio of 70:30 of acetonitrile to 10 mM ammonium phosphate
293 buffer (pH 2). A phenyl-hexyl stationary phase of 2.5 μm particle size and 4.6x100
294 diameter from XSelect® CSH™ (Waters Corporation, Massachusetts, USA) was
295 mounted as the HPLC column. The method was set to sustain a flowrate of 0.5 mL per
296 minute, with detection at an ultraviolet (UV) wavelength of 250 nm, using the Agilent
297 OpenLab software version 3.4 (Agilent Technologies AG, Santa Clara, USA). The
298 retention time obtained was 2.1 ± 0.1 min. The calibration curve was plotted using
299 samples diluted from a stock solution of 1 mg/mL of venetoclax in the mobile phase, to
300 give the concentrations 0.001-0.1 mg/mL. The lower limit of detection (LoD) on the
301 calibration curve was calculated to be 0.004 mg/mL, and the lower limit of quantification
302 (LoQ) on the calibration curve was calculated to be 0.01 mg/mL. The LoD was calculated
303 by dividing the standard deviation of the response by the slope of the standard curve and
304 multiplying the result by 3.3. The LoQ was calculated by multiplying the result of the
305 previously described division by 10. These were calculated according to the description
306 in the ICH Q2(R1) guidelines. The analysis was performed in triplicate. The data analysis
307 was performed using the Microsoft Excel data analysis tool pack (version 2016) and
308 GraphPad Prism software (version 10.0.2).

309 **2.6 Dispersion testing and droplet sizes of oil dispersions**

310 The dispersion tests were performed by diluting the samples to 1:100 v/v in
311 demineralized water. The samples were exposed to light shaking (by hand) before the
312 microscopic evaluation performed using polarized optical light microscopy (Model
313 DSX10-SZH, Olympus corporation, Tokyo, Japan). The diameters of 100 of the largest
314 visible spherical droplets were measured in different optical fields and used to plot a
315 distribution. 40x and 100x magnifications were used to study the systems.

316 **2.7 Physical solubility of surfactants in HDES**

317 The physical solubility of the surfactants in HDES was determined by adding 10, 20
318 and 30% w/w of the surfactants to the HDES and observing the physical state after 24 h
319 of stirring. If the solution was transparent with no microscopically visible particles after 24
320 h of mixing at 350 rpm (at ambient conditions), it was deemed dissolved.

321 **2.8 Determination of freezing points using differential scanning calorimetry (DSC)**

322 The freezing points of the samples with and without Tween 80 (10, 20, and 30%
323 w/w) and 70 mg/mL API were measured by weighing a few milligrams (3-10 mg) of the
324 samples into T_{zero} aluminum pans (TA instruments, Eschborn, Switzerland) sealed using
325 T_{zero} aluminum lids (TA instruments, Eschborn, Switzerland), and exposed to a cooling
326 ramp from 25°C to -15°C at 1°C/min at the nitrogen purge of 50 mL/min on the DSC
327 (Discovery DSC, TA Instruments, Eschborn, Switzerland). The onset point of the

328 **exothermic** peak was taken as the freezing point of the measured liquids. The analysis
329 was based on the TRIOS software (version 3.1.0.3538) complementary to the Discovery
330 DSC and the study was performed in triplicate.

331 **2.9 USP II dissolution test**

332 A triplicate standard USP II dissolution test was performed using the Pion
333 MacroFLUX™ dissolution instrument (Macroflux™, Pion Inc., Billerica, MA, USA) as a
334 detection device, connected to UV-probes (Pion Rainbow Dynamic Dissolution Monitor®,
335 Pion Inc., Billerica, MA, USA), submerged in the Hanson SR8-Plus dissolution bath
336 (Hanson Research, California, USA). Real-time (on-line) data on the released
337 concentrations of API were displayed on to the AuPRO software version 6.0.3.232, where
338 the data was further analyzed. The dissolution curves were obtained by measuring the
339 concentrations of venetoclax released from 1 mL of 70 mg/mL loaded formulations at the
340 UV-range of 337-357 nm, in 350 mL of FeSSIF-V2, at the stirring rate of 75 rpm and
341 temperature of 37°C over the course of 2 h. Note that the formulations tested were
342 prepared fresh and used within 24 h of production. FeSSIF-V2 was prepared according
343 to instructions provided on the biorelevant homepage (biorelevant.com) (Marques, 2004)
344 using a standard phosphate buffer base adjusted to pH 6.5 with 0.1 M sodium hydroxide
345 (Sigma-Aldrich, Steinheim, Germany). The standard curve was determined based on a
346 stock solution of 1 mg/mL of venetoclax in a solution of 10:90 v/v of glacial acetic acid to
347 acetonitrile, at concentration ranges of 2-40 µg/mL diluted in FeSSIF-V2. The apparent
348 supersaturations were then presented by dividing the API concentration obtained at 120
349 minutes of release by the solubility of venetoclax in FeSSIF-V2.

350 **2.10 Stability test - chemical degradation of venetoclax**

351 A triplicate stress test was performed in three batches of each formulation to
352 evaluate the stability of the HDES with 10, 20 and 30% w/w of added Tween 80 versus
353 the pure HDES. The API loadings corresponded to 70 mg/mL in all formulations. A volume
354 of 1 mL was transferred to a clear crimp-top hermetically sealed HPLC glass vial (ALWCSI
355 Technologies Co. Ltd., Zhejiang PR, China), sealed using silver rubber-septa crimp caps
356 (ALWCSI Technologies Co. Ltd., Zhejiang PR, China), and placed in the study condition
357 of 60% relative humidity (RH) at 25°C. The humidity was controlled using saturated salt
358 desiccators of sodium bromide (57.6% RH) placed in jars positioned in temperature-
359 regulated humidity chambers (Memmert GmbH + Co. KG, Schwabach, Germany). The
360 peak signal corresponding to the API was obtained using HPLC (section 2.5.1) and
361 compared at two time-points: the initial time-point before starting the stress test and the
362 second point after 2 weeks of stressing. The chromatograms were also monitored for the
363 appearance of additional peaks. Variations in the retention time of API-related peaks were
364 accepted up to ± 10%. Additionally, the samples were also studied for traces of
365 crystallinity using microscopy (Model DSX10-SZH, Olympus corporation, Tokyo, Japan).

366 **2.11 Statistical analysis and graphics using GraphPad Prism**

367 All statistical analyses were performed using GraphPad Prism (version 10.0.2,
368 GraphPad software, California, USA). **The one-way ANOVA calculations were**

369 complemented with either Tukey or Dunnett tests where necessary. The Tukey test was
370 employed when the ANOVA test compared different sets of means to each other, whilst
371 the Dunnett test was applied when the sets of means were to be compared to a single
372 mean value. The null hypotheses in the statistical tests presumed that the means of two
373 or more populations are equal, with a variation threshold (p -value) of 0.05. P -values below
374 0.05 resulted in the rejection of the null-hypothesis, demonstrating a significant difference
375 amongst a group of means.

376 All graphs and figures of the results obtained from all experiments were also
377 illustrated using the GraphPad prism program.

378 3 Results

379 The results section is divided into three main parts: 3.1, 3.2, and 3.3. The first
380 section characterizes the HDES itself with a model of its phase behavior. This section
381 concludes by studying venetoclax solubility in HDES as compared to other lipophilic
382 media and analyses the mixtures' molecular architecture with and without drug using
383 molecular dynamics (MD) simulations. Section 3.2 is about the impact of adding
384 surfactant (i.e., Tween 80) to the DES to study the performance of the final lipid-based
385 formulation. Finally, based on the findings in 3.2, an arbitrary loading concentration was
386 then used to characterize the dissolution of API from the formulations using the in-vitro
387 USP II dissolution setup.

388 3.1 HDES selection, characterisation, optimization, and API solubility

389 The HDES used in this study has been previously described outside the field of
390 pharmaceuticals by Florindo et al., 2018 as a liquid used for extracting bisphenol A (a
391 micropollutant) from aqueous environments (Florindo et al., 2018). The HDES is made of
392 a 1:2 molar ratio of dodecanoic acid to decanoic acid (Florindo et al., 2018). It can be
393 seen in figure 1 showing a clear homogenous liquid with the melting point of $19.70^{\circ}\text{C} \pm$
394 0.11°C , viscosity of $9.3 \pm 0.3 \text{ mPa}\cdot\text{s}$, density of $896.0 \pm 0.1 \text{ kg/m}^3$ and a water content
395 below 0.07% w/w. Dodecanoic acid (DoA) and decanoic acid (DeA) have both been
396 defined as pharmaceutically safe excipients, used for taste masking, emulsification, food
397 additives, lubricants or surfactants (Rowe et al., 1994). They are both medium-chain
398 saturated fatty acids, with a chain length of 10 carbons in the case of the decanoic acid
399 and 12 carbons in the dodecanoic acid (Rowe et al., 1994).

400

401 (Figure 1)

402

403 3.1.1 HDES characterization

404 The selected HDES is characterized using phase diagrams to establish the
405 thermodynamic behavior of the liquid. The ideal phase behavior was assessed using the
406 Schröder van Laar (SvL) equation (equation 1 with the activity coefficient of unity)

407 together with a solid-liquid line (SL-line) including UNIFAC activity coefficients (equation
408 1), referred to as the UNIFAC model. Finally, the experimentally obtained solid-liquid line
409 can be found overlaid in figure 2. The resulting eutectic points from figure 2 are reported
410 in table 1 with fusion properties taken from the literature. The melting point of the DeA
411 was set to 31.5°C (Hawley & Lewis, 2002), with an enthalpy of fusion of 29.4 kJ/mol
412 (Moreno et al., 2007). The melting point for DoA was found to be 43.2°C (Jiesheng et al.,
413 2016) and the enthalpy of fusion to be 36.7 kJ/mol (Moreno et al., 2007). These values
414 were used to plot the modelled systems, i.e., the ideal SvL and the UNIFAC model.

415

416 (Figure 2)

417

418 (Table 1)

419

420 The eutectic point in the ideal SvL system was only 1.12°C higher than that found
421 by the DSC experiments. The UNIFAC model resulted in a eutectic temperature only
422 0.03°C lower than the SvL value and was thus closer to the actual experimental value of
423 19.70°C ± 0.11°C. Accordingly, the UNIFAC model results in a DeA molar fraction around
424 0.05 units lower than the experimental molar fraction at the eutectic point. Hence, the SvL
425 molar fraction obtained at 0.02 units lower than the experimental molar fraction, was
426 closer to the experimentally obtained eutectic point (2:1 of DoA to DeA). Collectively the
427 results and the UNIFAC approximation agree in that no substantial deviance from ideal
428 mixing behavior was obtained.

429 3.1.2 Optimization of HDES as a lipid-based formulation (LBF)

430 The HDES showed highly hydrophobic characteristics as it did not spontaneously
431 form droplets upon dispersion in an aqueous medium. This can be seen in figure 3,
432 showing a droplet of HDES floating on top of the aqueous liquid.

433

434 (Figure 3)

435

436 To improve dispersion of HDES into water, several surfactants were examined.
437 The surfactants were assessed at the concentration of 10, 20, and 30% w/w of the HDES,
438 as described in section 2.7. The surfactants tested included Labrasol ALF (PEG-8 capric
439 glycerides), Labrafil M 2125 CS (corn oil PEG-6 esters), Labrafac lipophile WL 1349
440 (medium-chain TGs), Tween 80 (polysorbate 80), Gelucire 44/14 (lauroyl PEG-32
441 glycerides), Gelucire 48/16 (PEG-32 stearate), Soluplus®, and Poloxamer 188, of which
442 only the first four were soluble at these concentrations. These surfactants were then

443 selected for further testing and evaluation of aqueous dispersibility. The dispersibility of
444 the prepared mixtures of HDES with either Labrasol ALF, Labrafil M 2125 CS, Labrafac
445 lipophile WL 1349, or Tween 80 at the concentrations of 10, 20 and 30% w/w were tested
446 in aqueous medium according to the method described in section 2.6. They all resulted
447 in coarse emulsions upon dispersion and light shaking. The average droplet diameters of
448 the evaluated dispersions are outlined in table 2.

449

450 (Table 2)

451

452 The data was analyzed with statistical one-way ANOVA Dunnett testing,
453 comparing droplet diameters of the surfactant-containing samples to those of the pure
454 HDES with an average droplet diameter of $78.3 \mu\text{m} \pm 24.7 \mu\text{m}$. Accordingly, samples with
455 Tween 80 (polysorbate 80) were the only ones resulting in a significant drop in droplet
456 diameter. Therefore, HDES with either 10, 20, or 30% w/w of Tween 80 were selected as
457 the final LBF candidates. These all had a homogenous and transparent appearance.

458 3.1.3 Addition of API to HDES

459 Venetoclax solubility in the functional samples was determined according to the
460 methods described in section 2.5. It is noteworthy that adding a large excess of
461 venetoclax typically changed the HDES liquid samples into a paste by the end of the 24
462 h equilibration time. Hence, a trial-and-error method was applied to target an excess
463 concentration of venetoclax that would leave behind only a small residual amount of
464 dispersed API particles in the vials at the end of equilibration. The solubility values
465 obtained were then compared to those found in a long-chain triglyceride oil (sesame oil),
466 a medium-chain triglyceride (Miglyol® 812 N) and FeSSIF-V2. The selected oils were to
467 represent other classically used API-carrying oil phases in LBFs to have a solubility
468 reference. Table 3 shows that increased amounts of venetoclax can be dissolved in the
469 HDES compared to the reference oils tested. Nevertheless, the solubility of venetoclax
470 was higher in all the oils compared to the aqueous FeSSIF-V2 medium, which showed a
471 solubility value below the LoQ described in section 2.5.1. Based on the substantial
472 solubility improvement in the chosen HDES of DeA:DoA (2:1) compared to the other two
473 oils (i.e., sesame oil and Miglyol® 812 N), this new type of LBF was further investigated.

474

475 (Table 3)

476

477 3.1.3.1 Mechanistic study on molecular positioning of venetoclax in HDES

478 Molecular dynamics (MD) simulations were performed on the pure HDES
479 (DeA:DoA at the molar ratio of 2:1) and the HDES with 5% w/w of venetoclax, to study

480 the molecular architecture of the formulation mechanistically (see figure 4). The average
481 molecular interactions of the quadruplicate simulation runs are reported in table 4.

482

483 (Table 4)

484

485 (Figure 4)

486

487 The simulation showed that in total there were around 150-160 accepted and
488 donated hydrogen bonds and about 12'000 hydrophobic contact points between the pure
489 HDES components. Once 5% w/w of venetoclax was added, these values were reduced
490 to about 130-140 accepted hydrogen bonds and 140-150 donated hydrogen bonds,
491 resulting in ~11'000 hydrophobic contact points between the constituting components
492 (DeA and DoA) in the entire simplified model system. Furthermore, a statistical analysis
493 comparing the mean hydrogen bonding energies between the DeA and DoA molecules
494 showed a notable reduction (p -value < 0.0001) in the case of the venetoclax-containing
495 sample versus the pure HDES, going from 7179.1 kJ/mol in the pure HDES to 6195.0
496 kJ/mol in the HDES loaded with 5% w/w of venetoclax. The API showed a slight
497 preference for interactions with the DeA component compared to the DoA component, as
498 slightly higher hydrogen bonding and hydrophobic energies were observed between the
499 DeA with API (549.7 kJ/mol and 811.7 kJ/mol) as opposed to the DoA with API (263.9
500 kJ/mol and 430.6 kJ/mol) (p -value < 0.0001). In the entire simulated system, DeA and
501 venetoclax showed around 13 accepted and 16 donated hydrogen bonds with roughly
502 1000 hydrophobic contacts, whereas the DoA and venetoclax had about 4 accepted and
503 8 donated hydrogen bonds and of the order of 500 hydrophobic contacts. The API also
504 revealed some interactions with itself through hydrogen bonds, pi-pi interactions, and
505 cation pi interactions. However, these values were found to be substantially lower than
506 the interaction energies occurring between the API and the DES components. The
507 distribution of API appeared to be comparatively homogenous in the model system
508 indicating good solubilization without signs of phase separation from either the drug or
509 any other HDES component.

510 **3.2 Impact of Tween 80 on LBF drug solubility and release**

511 **3.2.1 Impact of Tween 80 on drug solubility in the formulation**

512 The solubility of venetoclax in the final formulation candidates was determined and
513 compared to the pure HDES as depicted in figure 5 and listed in table 5. To assess the
514 equilibration time, statistical evaluations of each of the formulations were performed using
515 Tukey and Dunnett ANOVA tests (section 2.11). Thus, after 72 h of stirring at 25°C,
516 equilibrium was reached except for the 30% w/w Tween 80, which varied significantly
517 from the values obtained at 24 and 48 h at 25°C. A reduction from 118.2 ± 4.3 mg/mL in
518 HDES to 89.8 ± 4.8 mg/mL in the 30% w/w Tween 80 sample was observed in the 72 h

519 equilibrated samples. Based on the data obtained, the final formulations were loaded with
520 70 mg/mL of API, representing an arbitrarily selected dose strength corresponding to a
521 drug-loading of 7.2% w/w in the pure HDES, 6.6% in the HDES formulation with 10% w/w
522 Tween 80, 5.9% w/w in the HDES with 20% w/w Tween 80, and 5.2% w/w in the HDES
523 with 30% w/w Tween 80.

524

525 (Figure 5)

526

527 (Table 5)

528

529 3.2.2 Impact of venetoclax on dispersibility of HDES with Tween 80

530 The impact of the added venetoclax on droplet diameter was studied in the LBF
531 formulations in absence and presence of different Tween 80 concentrations (Table 6). In
532 the case of the formulations containing Tween 80, adding venetoclax changed the
533 droplet-diameter reducing effect of the added surfactant, as described in section 3.1.2.
534 The droplet diameter changed to values comparable to that of the pure HDES with API,
535 and only the HDES with 30% w/w Tween 80 resulted in a smaller droplet size.

536

537 (Table 6)

538

539 3.2.3 Impact of Tween 80 and venetoclax on the freezing point of HDES

540 The freezing points were studied because the eutectic point of the DeA:DoA (2:1)
541 HDES was $19.7^{\circ}\text{C} \pm 0.1^{\circ}\text{C}$, and hence could crystallize at ambient conditions (Palmelund
542 et al., 2020). The acquired values are summarized in table 7.

543

544 (Table 7)

545

546 The addition of 10, and 20% w/w Tween 80 did not significantly change the freezing
547 point; a drop from $17.3^{\circ}\text{C} \pm 0.1^{\circ}\text{C}$ in the pure HDES to $15.4^{\circ}\text{C} \pm 0.7^{\circ}\text{C}$ in HDES with 30%
548 w/w of Tween 80 was observed. An additional drop in the freezing point was observed
549 once the API was added to the formulations of 20 and 30% w/w Tween 80, resulting in a
550 difference of -1.8°C and -3.1°C respectively compared to the HDES with API.

551 3.2.4 Impact of Tween 80 on preliminary stability testing of the formulations

552 The stability of the samples was determined according to the method described in
553 section 2.10. As presented in figure 6, the concentration of the API in the stressed
554 samples of 30% w/w Tween 80 deviated significantly after two weeks of storage.
555 However, no other peak was observed on the chromatograms, and the retention time of
556 the API-corresponding peak did not deviate. Additionally, no precipitates were observed
557 microscopically after the two-week stressing cycle.

558

559 (Figure 6)

560

561 3.3 In-vitro dissolution assessment using the USP II setup

562 The dissolution profiles of the prepared formulations, namely the pure HDES and
563 HDES with 10, 20, and 30% w/w Tween 80, with API-loading of 70 mg/mL can be seen
564 in figure 7. The figure shows higher concentrations released from the samples with higher
565 concentrations of Tween 80. The concentrations of API released after 120 mins of
566 dissolution are summarized in table 8.

567

568 (Figure 7)

569

570 (Table 8)

571

572 The surfactant enabled **apparent** supersaturation of API in the release medium,
573 FeSSIF-V2. Apparent supersaturations of 1.7, and 2.6 were seen for the 10% and 20%
574 w/w Tween 80 samples, whilst **apparent** supersaturations up to 3.1 were recorded for the
575 HDES with 30% w/w Tween 80. A lower apparent supersaturation of 1.1 was documented
576 in the pure HDES. The difference between each of the **estimated** supersaturation values
577 diminished with increasing Tween 80 concentrations, therefore a limit of supersaturation
578 was apparently given for increased surfactant concentrations.

579 4 Discussion

580 4.1 Utilization of HDES to formulate a highly lipophilic model compound

581 The scientific study of DES has been a thriving field in chemistry for a few years,
582 but only in recent years have these systems sparked a rising interest in delivering
583 nutraceuticals and drugs (Faggian et al., 2016; Fourmentin et al., 2021; Palmelund,

584 Eriksen, et al., 2021; Panbachi et al., 2023; Sut et al., 2017). A seminal study compared
585 drug solubility in different DES with values obtained in common pharmaceutical solvents
586 (Palmelund et al., 2019). The authors found a range of different solubility values, some
587 impressively high, but it was the specific chemistry of both vehicle and API that
588 determined the extent of drug solubilization. It seems that much pharmaceutical novelty
589 still remains to be uncovered and a recent example is the embedding of a polymeric-
590 precipitation inhibitor in a DES to obtain sustained drug supersaturation values on
591 aqueous dispersion of the formulation (Panbachi et al., 2023). For the present work,
592 hydrophobic systems, HDES were to be explored to formulate the highly lipophilic model
593 drug venetoclax. Although eutectic mixtures and DES have been used in chemical
594 engineering before (Florindo et al., 2018), a pharmaceutical application to formulate a
595 poorly water-soluble drugs are new to the best of our knowledge. Part of the research
596 question was to study such an HDES starting from the phase diagram to the drug
597 solubilising potential. A further aim was to get molecular insights into the structure of such
598 a system. Moreover, there was the biopharmaceutical perspective on how such a system
599 would disperse in aqueous medium and eventually add a surfactant, which would provide
600 a new kind of LBF with an HDES replacing a more traditional oily phase composed of
601 glycerides.

602 **4.2 In-silico versus experimental characterization of the HDES**

603 A majority of early published studies on DES presented formulations without
604 investigating their phase behavior. As a result of the present study, the thermodynamically
605 non-ideal behavior of the HDES was confirmed through a lower observed eutectic point
606 compared to that obtained in the modelled 'ideal' mixture following the Schröder van Laar
607 equation (SvL), as displayed in figure 2. The DeA:DoA (2:1) system has previously been
608 reported as a hydrophobic DES (HDES) in the work of Dwamena, 2019, yet the phase
609 diagram presented in the present pharmaceutical study aimed to provide a deeper
610 thermodynamic understanding of the system. The overall proximity of the computationally
611 predicted ideal eutectic point to the experimental eutectic point could imply that the HDES
612 behaved rather as a eutectic mixture instead of a true 'deep' eutectic mixture. However,
613 in the definitions of DES in the literature there is no clear threshold for the magnitude of
614 negative deviation of the eutectic point from ideal behavior (Abranches & Coutinho, 2023;
615 Hansen et al., 2021; Martins et al., 2019). The term DES or HDES is often broadly used
616 in applied sciences without knowledge of comparative ideal phase behavior; in the
617 present study, the 1.12°C lower experimental eutectic point was identified and the
618 DeA:DoA (2:1) was called a HDES in line with the pioneering work Florindo et al., 2018.

619 As for the prediction of DES behavior, the UNIFAC model performed similar to the
620 SvL model, predicting a eutectic temperature only 0.03°C closer to the experimental
621 value. However, the SvL model predicted a molar fraction that was slightly closer to the
622 experimental molar fraction. Despite the eutectic melting values being very similar to the
623 experimental output, the UNIFAC model was apparently not much more accurate than
624 the ideal SvL approach for the system studied. Overall, the precision of both models can
625 be viewed as acceptable. There are possible small errors from the fusion data obtained
626 from the literature and on the other hand, there is also the possibility that small
627 experimental errors occurred. Finally, pioneering work on UNIFAC modelling of

628 therapeutic DES already indicated that model precision depended to some extent on the
629 specific system studied. While the model precision in the present study was adequate for
630 the purpose of characterizing a fatty acid mixture, a main drawback of UNIFAC modelling
631 is generally the availability of group contributions and all possible interaction terms, which
632 generally limits current UNIFAC modelling of complex APIs.

633 The modelling of the phase diagram was complemented with MD simulations to
634 gain atomistic insights into the structure of the DES both as binary mixture of the fatty
635 acids as well as in the presence of the model drug venetoclax. The simulations were
636 based on an all-atom force field (GAFF2) (Wang et al., 2004) of the AMBER family of
637 potential energy functions. This type of force field has often been used to model DES as
638 a recent review indicated (Tolmachev et al., 2022). As a snapshot result of the
639 equilibration cycle at room temperature, figure 4 reveals a structure in accord with the
640 more recent view of DES as a chaotic 'hydrogen bond-alphabet-soup' (Ashworth et al.,
641 2016). Moreover, such high configuration randomness has also been observed in
642 previous MD DES simulations (Ashworth et al., 2016; Fourmentin et al., 2021). Since the
643 prepared HDES is made of fatty acids, a possible expectation was some laminar layering
644 of the alkyl chains to occur, as typically observed in fatty acid co-crystals (Prathapa et al.,
645 2018). However, figure 4 shows no traces of such ordered macrostructural configuration
646 of the liquid. Thus, the chaotic liquid structure of the DES was apparently favorable for
647 the two constituting components to achieve a high configurational entropy contribution to
648 the free energy of mixing.

649 As a result of added API, a decline in the occurrence of hydrogen bonds between
650 the HDES components (DeA and DoA) was observed. Venetoclax further decreased the
651 hydrophobic interactions of the interacting fatty acids (table 4) so the presence of this
652 external component in the HDES caused a moderate perturbation of the system. It is
653 noteworthy in this context that the solubility reported in this study is an 'apparent' solubility
654 value. This is because excess venetoclax within the system caused the liquid mixture to
655 morph into a coarse paste-like material. Since the solubilization of the APIs in DES
656 systems are dependent on the hydrogen-bond network within the DESs, it is critical that
657 the DES itself can sustain a sufficiently strong hydrogen bonding network in the presence
658 of the API (Palmelund et al., 2020). Therefore, an apparent maximum solubility may
659 represent a limiting drug concentration at which the DeA:DoA (2:1) HDES still has the
660 capacity to sustain structural intactness.

661 Apparently, drug solubilization of the HDES relies on the hydrogen bonds in the
662 system where some bonds with drug are often favorable regarding solvation capacity but
663 the network of such interactions between the DES components should not be overly
664 interrupted. Accordingly, good DES formulations are based on finely balanced
665 interactions and the case of venetoclax apparently showed more hydrophobic interactions
666 than hydrogen bonding with the DES components. The drug was interacting on the
667 average slightly more with the DeA than the DoA component, but this was likely due to
668 the shorter chain length of DeA resulting in a higher density of carboxylic groups to
669 interact. Venetoclax was further shown to interact with itself occasionally via hydrogen
670 bonds, hydrophobic interactions, pi-pi interactions, and proton-pi interactions. That said,
671 due to the much lower number of drug molecules in the simulation as compared to DES

672 components, these findings were not evaluated quantitatively and should be regarded as
673 qualitative information. This self-cohesion tendency of venetoclax underlines the
674 importance of excipient interactions, even more important for such a hydrophobic
675 compound in an aqueous environment on dispersion to keep the drug from precipitation
676 (Koehl et al., 2021).

677 **4.3 Use of the HDES as oil phase in lipid-based system**

678 As described in the introduction, venetoclax is a BCS class IV API, not meeting the
679 requirements of Lipinski's rule of 5 (Hartung et al., 2023). The high lipophilicity of
680 venetoclax comes with a problematically high crystal energy (Koehl et al., 2021) making
681 drug solubility even in hydrophobic solvents rather limited, which has led to previous
682 consideration of lipid-based suspension formulations and lipophilic salts (Koehl et al.,
683 2021, 2022). The present study interestingly revealed about a 100-fold increased
684 solubility in the DeA:DoA (2:1) HDES compared to that in sesame oil and Miglyol® 812
685 N. The latter two oils represent other classically employed long- and medium-chain
686 triglycerides in LBFs to solubilize API. Hence, a substantial solubility improvement was
687 attained compared to standard lipid phases for LBF, which raises the question of whether
688 the designation of the current system as a true DES or just a eutectic mixture has any
689 relevance from a practical pharmaceutical perspective. Thus, the selected HDES offers a
690 successful replacement for such oils as higher amounts of API could be solubilized in the
691 DES vehicle.

692 As LBF have to disperse adequately in the gastrointestinal tract (Porter et al.,
693 2008), initial aqueous dispersibility testing was conducted. Tween 80 was added to the
694 HDES vehicle as a surfactant at the concentrations of 10, 20, and 30% w/w. The addition
695 of the surfactant from the group of PEGylated sorbitan esters significantly reduced the
696 droplet diameter in comparison to other surfactants (refer to table 2) in an aqueous 1:100
697 v/v dispersion. The resulting emulsion can justify calling the initial surfactant containing
698 HDES a self-emulsifying drug delivery system (SEDDS) (Feeney et al., 2016). As the
699 composition of this type of system is new, there is no clear category assignment for the
700 lipid formulation classification system (Feeney et al., 2016; Pouton, 2006). Following the
701 addition of surfactant, the intactness of the solubilization capacity of the formulation was
702 re-examined. Indeed, higher amounts of the surfactant, specifically 30% w/w of Tween
703 80, resulted in comparatively lower solubilization of venetoclax in the formulations. This
704 is mainly because higher amounts of Tween 80 leave little compositional space for the
705 HDES in the given volume of the formulation. As a result, lower solubility was observed
706 due to less of the main solubilizing component that was apparently the HDES. This could
707 also explain the deviation in venetoclax concentrations recorded in the stressed HDES
708 samples with 30% w/w tween, indicating a potential start of nucleation of a solid
709 component.

710 In contrast to the lower API solubilization in the formulations, the higher
711 concentrations of incorporated Tween 80 resulted in higher concentrations of venetoclax
712 released into the aqueous medium (FeSSIF-V2) during the in-vitro release test (refer to
713 figure 7). Specifically, the dissolution of API from the HDES with 30% w/w Tween 80 was
714 the highest compared to the rest of the samples. The venetoclax concentration released

715 from the Tween 80-containing formulations into the FeSSIF-V2 dissolution medium
716 clearly exceeded the equilibrium concentration in pure medium, leading to apparent drug
717 supersaturation. An apparent supersaturation based on the biorelevant solubility can
718 provide first estimates of a final supersaturation in the release medium that may be also
719 influenced by the highly diluted excipients in the medium. In the present case, the latter
720 possible solubility effect is further diminished by a fast absorption of the fatty acids in vivo.

721 Apparent supersaturation is also often observed with other LBFs (Kuentz, 2019),
722 as it is triggered by fast dispersion and hence a partition process. The smaller droplets or
723 even colloids would result in enhanced release through increased surface area to volume
724 fractions of the formed droplets. It was interesting to observe that the impact of surfactant
725 concentration on droplet diameter was greatly affected by adding venetoclax. The high
726 lipophilicity of the venetoclax apparently altered the formulation's hydrophilic-lipophilic
727 balance (HLB), causing a change in diameter of the dispersed droplets (Wang et al.,
728 2023). The 30% w/w Tween 80 addition to HDES still resulted in slightly smaller droplet
729 sizes compared to the pure HDES with venetoclax but the effects of the surfactant in
730 reducing specific surface energy to promote dispersion were clearly limited by the
731 presence of drug. Although formulators generally target small droplet sizes on dispersion,
732 one has to add that there are no clear targets in what is desirable to achieve (Feeney et
733 al., 2016). Thus, improving a poorly dispersible oil phase by adding a surfactant is most
734 likely beneficial from a biopharmaceutical perspective. However, surfactant addition must
735 be balanced; it should not displace too much of the HDES in a composition to still achieve
736 excellent drug solvation capacity, as obtained in this study.

737 5 Conclusion

738 This study introduced a novel DES-based oil-phase for application in lipid-based
739 formulations. The selected DES was an HDES made of decanoic- and dodecanoic acid
740 in the molar ratio of 2:1. This HDES resulted in a eutectic temperature of $19.70^{\circ}\text{C} \pm 0.11^{\circ}\text{C}$
741 and the mixture dissolved an unprecedented amount of 118.2 ± 4.3 mg/mL of the highly
742 lipophilic drug venetoclax. The HDES performed 100-times better than the long- and
743 medium chain triglycerides sesame oil and Miglyol® 812 N in terms of solubilization. The
744 formulation was then optimized for better aqueous dispersion using Tween 80 as
745 surfactant in different concentrations. Although the surfactant concentration of 30% w/w
746 affected the solubilization capacity, no other significant change in the overall
747 characteristics of the HDES was observed. The formulation was finally in-vitro tested
748 using a compendial USP II release test where the resulting concentrations indicated that
749 the surfactant increased the released concentrations past the equilibrium concentration
750 of the API in the dissolution medium. Future biopharmaceutical testing may consider the
751 separate steps of gastric and intestinal release. Further testing under lipolysis conditions
752 is an option but only the surfactant can undergo lipolysis in the present case (Arnold et
753 al., 2012). There is surely more research in this field to be done but the present study
754 already suggests that using an HDES as lipophilic phase for LBF is a pertinent new drug
755 delivery approach. The high solvation capacity of HDESs observed is highly encouraging
756 for any further studies with LBFs to tackle the poor solubility of biopharmaceutically
757 challenging APIs.

758 **Declaration of competing interest**

759 The authors declare that they have no known competing financial interests or personal
760 relationships that could have appeared to influence the work reported in this paper.

761 **Author contribution**

762 Shaida Panbachi: Conceptualization, methodology, investigation, formal analysis,
763 validation, visualization, project administration, data curation, writing - original draft. Josef
764 Beranek: Supervisor, conceptualization, resources, writing - reviewing & editing. Martin
765 Kuentz: Supervisor, conceptualization, resources, molecular modelling, writing -
766 reviewing & editing.

767 **Data statement**

768 The presented experimental data can be obtained from the corresponding author on
769 request.

770 **Acknowledgments**

771 The author would like to thank the invaluable assistance and cooperation of Martina
772 Nehls, Laura Billingham, and Elilaha Sivasubramaniam on their valiant efforts and input
773 in the development of the excel file for modelling, and the screening and characterization
774 of the initial HDES prototypes. Andrew Brown is also acknowledged for his valued proof-
775 reading of the manuscript.

776 **Funding and role of funding source**

777 This work has received funding from the European Union's Horizon 2020 research and
778 innovation program the Marie Skłodowska-Curie grant agreement No 955756.
779 (InPharma). The funding source was not involved in the study design, in the collection,
780 analysis and interpretation of data, in the writing of the report, nor in the decision to submit
781 the article for publication.

782 **References**

- 783 Abdelquader, M. M., Li, S., Andrews, G. P., & Jones, D. S. (2023). Therapeutic deep
784 eutectic solvents: A comprehensive review of their thermodynamics, microstructure
785 and drug delivery applications. *European Journal of Pharmaceutics and*
786 *Biopharmaceutics*, *186*, 85–104. <https://doi.org/10.1016/J.EJPB.2023.03.002>
- 787 Abranches, D. O., & Coutinho, J. A. P. (2023). *Everything You Wanted to Know about*
788 *Deep Eutectic Solvents but Were Afraid to Be Told*. [https://doi.org/10.1146/annurev-](https://doi.org/10.1146/annurev-chembioeng)
789 [chembioeng](https://doi.org/10.1146/annurev-chembioeng)
- 790 Abranches, D. O., Martins, M. A. R., Silva, L. P., Schaeffer, N., Pinho, S. P., & Coutinho,
791 J. A. P. (2019). Phenolic hydrogen bond donors in the formation of non-ionic deep
792 eutectic solvents: the quest for type V DES. *Chemical Communications*, *55*(69),
793 10253–10256. <https://doi.org/10.1039/C9CC04846D>
- 794 Abusleme, J. A., & Vera, J. H. (1985). The quasi-chemical group solution theory for
795 organic mixtures. *Fluid Phase Equilibria*, *22*(2), 123–138.
796 [https://doi.org/10.1016/0378-3812\(85\)85015-9](https://doi.org/10.1016/0378-3812(85)85015-9)
- 797 Arnold, Y. E., Imanidis, G., & Kuentz, M. (2012). In vitro digestion kinetics of excipients
798 for lipid-based drug delivery and introduction of a relative lipolysis half life. *Drug*
799 *Development and Industrial Pharmacy*, *38*(10), 1262–1269.
800 <https://doi.org/10.3109/03639045.2011.645834>
- 801 Ashworth, C. R., Matthews, R. P., Welton, T., & Hunt, P. A. (2016). Doubly ionic hydrogen
802 bond interactions within the choline chloride-urea deep eutectic solvent †. *Phys.*
803 *Chem. Chem. Phys*, *18*, 18145. <https://doi.org/10.1039/c6cp02815b>
- 804 Benvenuti, L., Zielinski, A. A. F., & Ferreira, S. R. S. (2019). Which is the best food
805 emerging solvent: IL, DES or NADES? *Trends in Food Science and Technology*, *90*,
806 133–146. <https://doi.org/10.1016/J.TIFS.2019.06.003>
- 807 Chakraborty, S., Chormale, J. H., & Bansal, A. K. (2021). Deep eutectic systems: An
808 overview of fundamental aspects, current understanding and drug delivery
809 applications. *International Journal of Pharmaceutics*, *610*, 121203.
810 <https://doi.org/10.1016/J.IJPHARM.2021.121203>
- 811 Dai, Y., van Spronsen, J., Witkamp, G. J., Verpoorte, R., & Choi, Y. H. (2013). Natural
812 deep eutectic solvents as new potential media for green technology. *Analytica*
813 *Chimica Acta*, *766*, 61–68. <https://doi.org/10.1016/J.ACA.2012.12.019>
- 814 DeGoey, D. A., & Cox, P. B. (2021). Drug Discovery Beyond the Rule of Five. *Burger's*
815 *Medicinal Chemistry and Drug Discovery*, 1–35.
816 <https://doi.org/10.1002/0471266949.BMC258>

- 817 Deiters, U. K. (2012). The isothermal van't Hoff equation for phase equilibria—A forgotten
818 relation? *Fluid Phase Equilibria*, 336, 22–27.
819 <https://doi.org/10.1016/J.FLUID.2012.08.028>
- 820 Dwamena, A. K. (2019). Recent Advances in Hydrophobic Deep Eutectic Solvents for
821 Extraction. *Separations 2019, Vol. 6, Page 9, 6(1), 9.*
822 <https://doi.org/10.3390/SEPARATIONS6010009>
- 823 Emami Riedmaier, A., Lindley, D. J., Hall, J. A., Castleberry, S., Slade, R. T., Stuart, P.,
824 Carr, R. A., Borchardt, T. B., Bow, D. A. J., & Nijsen, M. (2018). Mechanistic
825 Physiologically Based Pharmacokinetic Modeling of the Dissolution and Food Effect
826 of a Biopharmaceutics Classification System IV Compound—The Venetoclax Story.
827 *Journal of Pharmaceutical Sciences*, 107(1), 495–502.
828 <https://doi.org/10.1016/J.XPHS.2017.09.027>
- 829 Faggian, M., Sut, S., Perissutti, B., Baldan, V., Grabnar, I., & Dall'acqua, S. (2016).
830 *molecules Natural Deep Eutectic Solvents (NADES) as a Tool for Bioavailability*
831 *Improvement: Pharmacokinetics of Rutin Dissolved in Proline/Glycine after Oral*
832 *Administration in Rats: Possible Application in Nutraceuticals.*
833 <https://doi.org/10.3390/molecules21111531>
- 834 Feeney, O. M., Crum, M. F., McEvoy, C. L., Trevaskis, N. L., Williams, H. D., Pouton, C.
835 W., Charman, W. N., Bergström, C. A. S., & Porter, C. J. H. (2016). 50 years of oral
836 lipid-based formulations: Provenance, progress and future perspectives. *Advanced*
837 *Drug Delivery Reviews*, 101, 167–194. <https://doi.org/10.1016/J.ADDR.2016.04.007>
- 838 Florindo, C., Romero, L., Rintoul, I., Branco, L. C., & Marrucho, I. M. (2018). From Phase
839 Change Materials to Green Solvents: Hydrophobic Low Viscous Fatty Acid-Based
840 Deep Eutectic Solvents. *ACS Sustainable Chemistry and Engineering*, 6(3), 3888–
841 3895. <https://doi.org/10.1021/ACSSUSCHEMENG.7B04235>
- 842 Fourmentin, S., Costa Gomes, M., & Lichtfouse, E. (2021). *Deep eutectic solvents for*
843 *medicine, gas solubilization and extraction of natural substances.* 312.
- 844 Fredenslund, A., Jones, R. L., & Prausnitz, J. M. (1975). Group-contribution estimation of
845 activity coefficients in nonideal liquid mixtures. *Aiche Journal*, 21(6), 1086–1099.
846 <https://doi.org/10.1002/AIC.690210607>
- 847 Ghaedi, H., Ayoub, M., Sufian, S., Hailegiorgis, S. M., Murshid, G., & Khan, S. N. (2018).
848 Thermal stability analysis, experimental conductivity and pH of phosphonium-based
849 deep eutectic solvents and their prediction by a new empirical equation. *The Journal*
850 *of Chemical Thermodynamics*, 116, 50–60.
851 <https://doi.org/10.1016/J.JCT.2017.08.029>
- 852 Hansen, B. B., Spittle, S., Chen, B., Poe, D., Zhang, Y., Klein, J. M., Horton, A., Adhikari,
853 L., Zelovich, T., Doherty, B. W., Gurkan, B., Maginn, E. J., Ragauskas, A., Dadmun,
854 M., Zawodzinski, T. A., Baker, G. A., Tuckerman, M. E., Savinell, R. F., & Sangoro,
855 J. R. (2021). Deep Eutectic Solvents: A Review of Fundamentals and Applications.

- 856 *Chemical Reviews*, 121(3), 1232–1285.
857 <https://doi.org/10.1021/acs.chemrev.0c00385>
- 858 Hartung, I. V., Huck, B. R., & Crespo, A. (2023). Rules were made to be broken. *Nature*
859 *Reviews Chemistry* 2023 7:1, 7(1), 3–4. [https://doi.org/10.1038/s41570-022-00451-](https://doi.org/10.1038/s41570-022-00451-0)
860 0
- 861 Hawley, G. G. (Gessner G., & Lewis, R. J. (2002). *Hawley's condensed chemical*
862 *dictionary*. 1223.
- 863 Huber, V., Hioe, J., Touraud, D., & Kunz, W. (2022). Uncovering the curcumin
864 solubilization ability of selected natural deep eutectic solvents based on quaternary
865 ammonium compounds. *Journal of Molecular Liquids*, 361, 119661.
866 <https://doi.org/10.1016/J.MOLLIQ.2022.119661>
- 867 (ICH Topic Q 2 (R1) *Validation of Analytical Procedures: Text and Methodology Step 5*
868 *NOTE FOR GUIDANCE ON VALIDATION OF ANALYTICAL PROCEDURES: TEXT*
869 *AND METHODOLOGY* (CPMP/ICH/381/95) APPROVAL BY CPMP November 1994
870 DATE FOR COMING INTO OPERATION, 1995)
- 871 Jakalian, A., Jack, D. B., & Bayly, C. I. (2002). Fast, efficient generation of high-quality
872 atomic charges. AM1-BCC model: II. Parameterization and validation. *Journal of*
873 *Computational Chemistry*, 23(16), 1623–1641. <https://doi.org/10.1002/JCC.10128>
- 874 Jeliński, T., Przybyłek, M., & Cysewski, P. (2019). *Natural Deep Eutectic Solvents as*
875 *Agents for Improving Solubility, Stability and Delivery of Curcumin*.
876 <https://doi.org/10.1007/s11095-019-2643-2>
- 877 Jiasheng, L., Yuanyuan, Y., & Xiang, H. (2016). Research on the preparation and
878 properties of lauric acid/expanded perlite phase change materials. *Energy and*
879 *Buildings*, 110, 108–111. <https://doi.org/10.1016/J.ENBUILD.2015.10.043>
- 880 Koehl, N. J., Henze, L. J., Bennett-Lenane, H., Faisal, W., Price, D. J., Holm, R., Kuentz,
881 M., & Griffin, B. T. (2021). In Silico, in Vitro, and in Vivo Evaluation of Precipitation
882 Inhibitors in Supersaturated Lipid-Based Formulations of Venetoclax. *Molecular*
883 *Pharmaceutics*, 18(6), 2174–2188.
884 https://doi.org/10.1021/ACS.MOLPHARMACEUT.0C00645/ASSET/IMAGES/LARGE/MP0C00645_0006.JPEG
885
- 886 Koehl, N. J., Henze, L. J., Holm, R., Kuentz, M., Keating, J. J., De Vijlder, T., Marx, A., &
887 Griffin, B. T. (2022). Lipophilic Salts and Lipid-Based Formulations for Bridging the
888 Food Effect Gap of Venetoclax. *Journal of Pharmaceutical Sciences*, 111(1), 164–
889 174. <https://doi.org/10.1016/J.XPHS.2021.09.008>
- 890 Koehl, N. J., Holm, R., Kuentz, M., & Griffin, B. T. (2019). New Insights into Using Lipid
891 Based Suspensions for “Brick Dust” Molecules: Case Study of Nilotinib.
892 *Pharmaceutical Research*, 36(4). <https://doi.org/10.1007/S11095-019-2590-Y>

- 893 Krieger, E., & Vriend, G. (2014). YASARA View - molecular graphics for all devices - from
894 smartphones to workstations. *Bioinformatics (Oxford, England)*, *30*(20), 2981–2982.
895 <https://doi.org/10.1093/BIOINFORMATICS/BTU426>
- 896 Kuentz, M. (2019). Drug supersaturation during formulation digestion, including real-time
897 analytical approaches. *Advanced Drug Delivery Reviews*, *142*, 50–61.
898 <https://doi.org/10.1016/J.ADDR.2018.11.003>
- 899 Li, Z., & Lee, P. I. (2016). Investigation on drug solubility enhancement using deep
900 eutectic solvents and their derivatives. *International Journal of Pharmaceutics*,
901 *505*(1–2), 283–288. <https://doi.org/10.1016/J.IJPHARM.2016.04.018>
- 902 Liu, Y., Friesen, J. B., McAlpine, J. B., Lankin, D. C., Chen, S.-N., & Pauli, G. F. (2018).
903 Natural Deep Eutectic Solvents: Properties, Applications, and Perspectives. *Journal*
904 *of Natural Products*, *81*(3), 679–690. <https://doi.org/10.1021/acs.jnatprod.7b00945>
- 905 Marques, M. (2004). Dissolution media simulating fasted and fed states. *Dissolution*
906 *Technologies*, *11*(2), 16. <https://doi.org/10.14227/DT110204P16>
- 907 Martins, M. A. R., Pinho, S. P., & Coutinho, J. A. P. (2019). Insights into the Nature of
908 Eutectic and Deep Eutectic Mixtures. *Journal of Solution Chemistry*, *48*(7), 962–982.
909 <https://doi.org/10.1007/s10953-018-0793-1>
- 910 Moreno, E., Cordobilla, R., Calvet, T., Cuevas-Diarte, M. A., Gbabode, G., Negrier, P.,
911 Mondieig, D., & Oonk, H. A. J. (2007). Polymorphism of even saturated carboxylic
912 acids from n-decanoic to n-eicosanoic acid. *New Journal of Chemistry*, *31*(6), 947–
913 957. <https://doi.org/10.1039/B700551B>
- 914 Morrison, H. G., Sun, C. C., & Neervannan, S. (2009). Characterization of thermal
915 behavior of deep eutectic solvents and their potential as drug solubilization vehicles.
916 *International Journal of Pharmaceutics*, *378*(1–2), 136–139.
917 <https://doi.org/10.1016/J.IJPHARM.2009.05.039>
- 918 Oyou, F., Toncheva, A., Henríquez, L. C., Grougnet, R., Laoutid, F., Mignet, N.,
919 Alhareth, K., & Corvis, Y. (2023). Deep Eutectic Solvents: An Eco-friendly Design for
920 Drug Engineering. *ChemSusChem*, *16*(20), e202300669.
921 <https://doi.org/10.1002/CSSC.202300669>
- 922 Palmelund, H., Andersson, M. P., Asgreen, C. J., Boyd, B. J., Rantanen, J., & Löbmann,
923 K. (2019). Tailor-made solvents for pharmaceutical use? Experimental and
924 computational approach for determining solubility in deep eutectic solvents (DES).
925 *International Journal of Pharmaceutics: X*, *1*, 100034.
926 <https://doi.org/10.1016/J.IJPX.2019.100034>
- 927 Palmelund, H., Boyd, B. J., Rantanen, J., & Löbmann, K. (2020). Influence of water of
928 crystallization on the ternary phase behavior of a drug and deep eutectic solvent.
929 *Journal of Molecular Liquids*, *315*, 113727.
930 <https://doi.org/10.1016/J.MOLLIQ.2020.113727>

- 931 Palmelund, H., Eriksen, J. B., Bauer-Brandl, A., Rantanen, J., & Löbmann, K. (2021).
932 Enabling formulations of aprepitant: in vitro and in vivo comparison of
933 nanocrystalline, amorphous and deep eutectic solvent based formulations.
934 *International Journal of Pharmaceutics*: X, 3, 100083.
935 <https://doi.org/10.1016/J.IJPX.2021.100083>
- 936 Palmelund, H., Rantanen, J., & Löbmann, K. (2021). Deliquescence Behavior of Deep
937 Eutectic Solvents. *Applied Sciences*, 11, 1601. <https://doi.org/10.3390/app11041601>
- 938 Panbachi, S., Beranek, J., & Kuentz, M. (2023). Polymer-embedded deep eutectic
939 solvents (PEDES) as a novel bio-enabling formulation approach. *European Journal*
940 *of Pharmaceutical Sciences*, 186, 106463.
941 <https://doi.org/10.1016/J.EJPS.2023.106463>
- 942 Porter, C. J. H., Pouton, C. W., Cuine, J. F., & Charman, W. N. (2008). Enhancing
943 intestinal drug solubilisation using lipid-based delivery systems. *Advanced Drug*
944 *Delivery Reviews*, 60(6), 673–691. <https://doi.org/10.1016/J.ADDR.2007.10.014>
- 945 Pouton, C. W. (2006). Formulation of poorly water-soluble drugs for oral administration:
946 Physicochemical and physiological issues and the lipid formulation classification
947 system. *European Journal of Pharmaceutical Sciences*, 29(3–4), 278–287.
948 <https://doi.org/10.1016/J.EJPS.2006.04.016>
- 949 Prathapa, S. J., Slabbert, C., Fernandes, M. A., & Lemmerer, A. (2018). Structure
950 determination of fatty acid ester biofuels via in situ cryocrystallisation and single
951 crystal X-ray diffraction. *CrystEngComm*, 21(1), 41–52.
952 <https://doi.org/10.1039/C8CE01673A>
- 953 Prigogine, I., & Defay, R. (1954). Chemical Thermodynamics: Treatise on
954 Thermodynamics Based on Methods of Gibbs and De Donder. In D. H. Everett (Ed.),
955 *Chemical Thermodynamics: Vol. I*. Longmans Green & Co Ltd.
956 <https://archive.org/details/chemicalthermody0000ipri>
- 957 Ramón, D. J., & Guillena, G. (2019). Deep eutectic solvents: Synthesis, properties, and
958 applications. *Deep Eutectic Solvents: Synthesis, Properties, and Applications*, 1–
959 370. <https://doi.org/10.1002/9783527818488>
- 960 Rowe, R., Sheskey, P., & Quinn, M. E. (1994). *Handbook of Pharmaceutical Excipients*.
- 961 Shah, V. P., & Amidon, G. L. (2014). G.L. Amidon, H. Lennernas, V.P. Shah, and J.R.
962 Crison. A theoretical basis for a biopharmaceutic drug classification: The correlation
963 of in vitro drug product dissolution and in vivo bioavailability, *Pharm Res* 12, 413-
964 420, 1995-Backstory of BCS. *AAPS Journal*, 16(5), 894–898.
965 <https://doi.org/10.1208/S12248-014-9620-9/METRICS>
- 966 Skjold-Jorgensen, S., Kolbe, B., Gmehling, J., & Rasmussen, P. (1979). Vapor-Liquid
967 Equilibria by UNIFAC Group Contribution. Revision and Extension. *Industrial &*

- 968 *Engineering Chemistry Process Design and Development*, 18(4), 714–722.
969 <https://doi.org/10.1021/i260072a024>
- 970 Sut, S., Faggian, M., Baldan, V., Poloniato, G., Castagliuolo, I., Grabnar, I., Perissutti, B.,
971 Brun, P., Maggi, F., Voinovich, D., Peron, G., & Dall, S. (2017). *molecules Natural*
972 *Deep Eutectic Solvents (NADES) to Enhance Berberine Absorption: An In Vivo*
973 *Pharmacokinetic Study*. <https://doi.org/10.3390/molecules22111921>
- 974 Tolmachev, D., Lukasheva, N., Ramazanov, R., Nazarychev, V., Borzdun, N., Volgin, I.,
975 Andreeva, M., Glova, A., Melnikova, S., Dobrovskiy, A., Silber, S. A., Larin, S., de
976 Souza, R. M., Ribeiro, M. C. C., Lyulin, S., & Karttunen, M. (2022). Computer
977 Simulations of Deep Eutectic Solvents: Challenges, Solutions, and Perspectives.
978 *International Journal of Molecular Sciences*, 23(2).
979 <https://doi.org/10.3390/IJMS23020645>
- 980 Umerska, A., Bialek, K., Zotova, J., Skotnicki, M., & Tajber, L. (2020). Anticrystal
981 engineering of ketoprofen and ester local anesthetics: Ionic liquids or deep eutectic
982 mixtures? *Pharmaceutics*, 12(4).
983 <https://doi.org/10.3390/PHARMACEUTICS12040368>
- 984 Van Osch, D. J. G. P., Dietz, C. H. J. T., Warrag, S. E. E., & Kroon, M. C. (2020). The
985 Curious Case of Hydrophobic Deep Eutectic Solvents: A Story on the Discovery,
986 Design, and Applications. *ACS Sustainable Chemistry and Engineering*, 8(29),
987 10591–10612.
988 [https://doi.org/10.1021/ACSSUSCHEMENG.0C00559/ASSET/IMAGES/MEDIUM/S](https://doi.org/10.1021/ACSSUSCHEMENG.0C00559/ASSET/IMAGES/MEDIUM/SC0C00559_0005.GIF)
989 [C0C00559_0005.GIF](https://doi.org/10.1021/ACSSUSCHEMENG.0C00559/ASSET/IMAGES/MEDIUM/SC0C00559_0005.GIF)
- 990 Wang, J., Wolf, R. M., Caldwell, J. W., Kollman, P. A., & Case, D. A. (2004). Development
991 and testing of a general amber force field. *Journal of Computational Chemistry*, 25(9),
992 1157–1174. <https://doi.org/10.1002/JCC.20035>
- 993 Wang, L., & Meng, D. (2010). Fatty acid eutectic/polymethyl methacrylate composite as
994 form-stable phase change material for thermal energy storage. *Applied Energy*,
995 87(8), 2660–2665. <https://doi.org/10.1016/J.APENERGY.2010.01.010>
- 996 Wolbert, F., Brandenbusch, C., & Sadowski, G. (2019). Selecting Excipients Forming
997 Therapeutic Deep Eutectic Systems-A Mechanistic Approach. *Molecular*
998 *Pharmaceutics*, 16. <https://doi.org/10.1021/acs.molpharmaceut.9b00336>
- 999 Zainal-Abidin, M. H., Hayyan, M., & Wong, W. F. (2021). Hydrophobic deep eutectic
1000 solvents: Current progress and future directions. *Journal of Industrial and*
1001 *Engineering Chemistry*, 97, 142–162. <https://doi.org/10.1016/J.JIEC.2021.03.011>
- 1002 Zhou, K., & Liu, B. (2022). Control techniques of molecular dynamics simulation.
1003 *Molecular Dynamics Simulation*, 67–96. [https://doi.org/10.1016/B978-0-12-816419-](https://doi.org/10.1016/B978-0-12-816419-8.00008-8)
1004 [8.00008-8](https://doi.org/10.1016/B978-0-12-816419-8.00008-8)
- 1005

Journal Pre-proofs

1007 **Figure captions**

1008

1009 **Figure 1.** Pure hydrophobic deep eutectic solvent (HDES), made of decanoic acid and
1010 dodecanoic acid at the molar ratio of 2:1.

1011

1012 **Figure 2.** Modelled solid-liquid lines (SL-line) and eutectic temperatures (eut. temp.)
1013 found through melting points calculated by the Schröder van Laar (SvL) equation,
1014 consideration of UNIFAC activity coefficients in equation 1, overlaid with the experimental
1015 thermoanalytical values (n=3, mean \pm SD).

1016

1017 **Figure 3.** Pure HDES dispersed in water at 1:100 v/v. Arrow pointing at the floating droplet
1018 of the HDES on top of the water.

1019

1020 **Figure 4.** Snapshot images following equilibration at room temperature HDES
1021 components are depicted as tubes- and API as ball-and-stick model. The tubes model
1022 shows DeA acid in blue, whilst the DoA is given without altered standard colors (i.e.,
1023 turquoise for carbons). The molecular surface of the DES components is shown in both
1024 images to mark the solubilizing environment of the API.

1025

1026 **Figure 5.** Bar chart of venetoclax solubilities (mg/mL) in HDES and HDES with 10, 20,
1027 and 30% w/w Tween 80 at 25°C after 24, 48 and 72 h and 37°C after 24 h (n=3, mean \pm
1028 SD).

1029

1030 **Figure 6.** Change in the concentration of API in stressed samples at the initial time point
1031 (t_0) and after two weeks ($t_0 + 2$ weeks). Values are representative of the concentration
1032 change (chemical degradation) of the API in the samples (n=3, mean \pm SD).

1033

1034 **Figure 7.** In-vitro USP II dissolution concentrations of 70 mg venetoclax from 1 mL of
1035 DeA:DoA (2:1) (HDES), and HDES with 10, 20, and 30% w/w of Tween 80 in 350 mL
1036 FeSSIF-V2, at 37°C over 120 min (n=3, mean \pm SD). The red dashed line refers to the
1037 equilibrium solubility of venetoclax in FeSSIF-V2.

1038

1039

1040

1041

Journal Pre-proofs

1042 **Tables**

1043

1044 **Table 1.** Summary of eutectic points obtained from the modelled phase diagrams of
 1045 Schröder van Laar solid-liquid line (activity coefficient of unity) and the modelled UNIFAC
 1046 activity coefficients in equation 1 with experimental values obtained from DSC (n=3, mean
 1047 \pm SD).

Model	Eutectic point	
	Molar fraction, DeA:DoA	Temperature
Schröder van Laar (ideal)	0.65:0.35	20.82°C
UNIFAC	0.62:0.38	20.79°C
Experimental	0.67:0.33	19.70°C \pm 0.11°C

1048

1049

1050

1051 **Table 1.** Overview of the droplet diameters of the HDES with 10, 20, and 30% w/w of the
 1052 different surfactants.

Surfactant concentration	Droplet diameter, μm			
	Labrafac lipophile WL 1349	Labrafil M 2125 CS	Labrasol ALF	Tween 80
10% w/w	86.7 \pm 54.7	44.2 \pm 18.0	47.8 \pm 31.4	12.4 \pm 5.6
20% w/w	86.2 \pm 30.7	42.0 \pm 18.1	36.3 \pm 13.2	7.4 \pm 1.7
30% w/w	73.0 \pm 41.1	58.7 \pm 24.1	32.5 \pm 9.7	9.5 \pm 4.1

1053

1054

1055

1056 **Table 3.** Solubility of venetoclax in HDES versus other media, including sesame oil (long
1057 chain triglyceride), Miglyol® 812 N, and FeSSIF-V2 (n=3, mean \pm SD).

Solubilising medium	Venetoclax solubility at 25°C after 72 h
HDES (DeA:DoA, 2:1)	118.2 \pm 4.3 mg/mL
Sesame oil	5.3 \pm 0.1 mg/mL
Miglyol® 812 N	1.30 \pm 0.01 mg/mL
FeSSIF-V2	< LoQ (9.4 \cdot 10 ⁻³ \pm 0.6 \cdot 10 ⁻³ mg/mL)

1058

1059

1060

1061 **Table 4.** Overview of interaction energies obtained through the 200 ps sampling at 298 K
 1062 (second cycle) simulations in samples with 5% w/w API versus the interaction between
 1063 the DeA and DoA in the pure HDES (without API) shown in the first row (n=4, mean \pm
 1064 SD).

Molecular interaction energies, kJ/mol				
Interaction type	Hydrogen bonding	Hydrophobic	Pi-Pi	Cation-pi
DeA with DoA (without API)	7179.1 \pm 283.9	9454.0 \pm 79.3	-	-
DeA with DoA (with 5% w/w API)	6195.0 \pm 514.1	9021.7 \pm 330.6	-	-
DeA with API	549.7 \pm 50.4	811.7 \pm 73.4	-	-
DoA with API	263.9 \pm 24.0	430.6 \pm 40.0	-	-
API with API	117.2 \pm 16.7	326.4 \pm 24.1	52.9 \pm 9.1	24.9 \pm 6.4

1065

1066

1067

1068 **Table 5.** Overview of venetoclax solubilities (mg/mL) in HDES and with added 10, 20,
 1069 and 30% w/w Tween 80 at 25°C after 24, 48 and 72 h and 37°C after 24 h (n=3, mean \pm
 1070 SD).

Venetoclax solubility (mg/mL) in the LBF mixtures				
Formulation	25°C	25°C	25°C	37°C
	24 h	48 h	72 h	24 h
HDES	100.6 \pm 3.2	118.7 \pm 0.7	118.2 \pm 4.3	118.9 \pm 2.0
HDES + 10% w/w Tween 80	104.1 \pm 8.2	107.6 \pm 2.5	103.9 \pm 9.2	111.6 \pm 1.0
HDES + 20% w/w Tween 80	109.0 \pm 7.2	110.0 \pm 4.3	111.3 \pm 9.5	105.9 \pm 1.7
HDES + 30% w/w Tween 80	102.5 \pm 6.6	98.6 \pm 1.2	89.8 \pm 4.8	57.1 \pm 1.7

1071

1072

1073

1074 **Table 6.** Change in droplet diameter in the formulations with and without API (n=3, mean
 1075 \pm SD).

Formulation	Droplet diameter, μm	
	without API	with 70 mg/mL API
HDES	78.3 \pm 24.7	45.5 \pm 33.5
HDES + 10% w/w Tween 80	12.4 \pm 5.6	44.1 \pm 29.8
HDES + 20% w/w Tween 80	7.4 \pm 1.7	48.2 \pm 28.7
HDES + 30% w/w Tween 80	9.5 \pm 4.1	33.9 \pm 17.5

1076

1077

1078

1079 **Table 7.** Overview of freezing points of the HDES with 10, 20, 30% surfactant, with and
1080 without 70 mg/mL of venetoclax (n=3, mean \pm SD).

Formulation	Freezing point, °C	
	without API	with 70 mg/mL API
HDES	17.3 \pm 0.1	16.8 \pm 0.4
HDES + 10 % w/w Tween 80	18.0 \pm 0.1	16.0 \pm 0.6
HDES + 20 % w/w Tween 80	17.2 \pm 0.4	15.0 \pm 0.4
HDES + 30 % w/w Tween 80	15.4 \pm 0.7	13.7 \pm 0.4

1081

1082

1083

1084 **Table 8.** Overview of dissolved concentration of venetoclax recorded at 120 min (n=3,
1085 mean \pm SD).

Formulation	Concentration of dissolved API, $\mu\text{g/mL}$
HDES	11.3 \pm 1.5
HDES+10% w/w Tween 80	17.5 \pm 2.2
HDES+20% w/w Tween 80	27.5 \pm 1.4
HDES+30% w/w Tween 80	32.0 \pm 0.8

1086

1087

1088

1089 Highlights

- 1090 • A hydrophobic deep eutectic solvent (HDES) is developed as a novel oil phase
1091 for LBFs
- 1092 • Phase diagrams are modeled to describe the thermodynamic behavior of the
1093 HDES
- 1094 • Molecular dynamics simulations are performed to examine the formulation
1095 architecture
- 1096 • The HDES solubilized more venetoclax compared to conventional oil-phase
1097 candidates
- 1098 • Combined with Tween 80, the HDES resulted in supersaturated venetoclax
1099 release

1100

1101 **Table 1.** Summary of eutectic points obtained from the modelled phase diagrams of
1102 Schröder van Laar solid-liquid line (activity coefficient of unity) and the modelled UNIFAC
1103 activity coefficients in equation 1 with experimental values obtained from DSC (n=3, mean
1104 \pm SD).

Model

Eutectic point

	Molar fraction, DeA:DoA	Temperature
Schröder van Laar (ideal)	0.65:0.35	20.82°C
UNIFAC	0.62:0.38	20.79°C
Experimental	0.67:0.33	19.70°C ± 0.11°C

1105

1106

1107 **Table 2.** Overview of the droplet diameters of the HDES with 10, 20, and 30% w/w of the
 1108 different surfactants.

1109

Surfactant concentration	Droplet diameter, μm			
	Labrafac lipophile WL 1349	Labrafil M 2125 CS	Labrasol ALF	Tween 80
10% w/w	86.7 ± 54.7	44.2 ± 18.0	47.8 ± 31.4	12.4 ± 5.6
20% w/w	86.2 ± 30.7	42.0 ± 18.1	36.3 ± 13.2	7.4 ± 1.7
30% w/w	73.0 ± 41.1	58.7 ± 24.1	32.5 ± 9.7	9.5 ± 4.1

1110

1111

1112

1113

1114

1115 **Table 3.** Solubility of venetoclax in HDES versus other media, including sesame oil (long
1116 chain triglyceride), Miglyol® 812 N, and FeSSIF-V2 (n=3, mean \pm SD).

Solubilising medium	Venetoclax solubility at 25°C after 72 h
HDES (DeA:DoA, 2:1)	118.2 \pm 4.3 mg/mL
Sesame oil	5.3 \pm 0.1 mg/mL
Miglyol® 812 N	1.30 \pm 0.01 mg/mL
FeSSIF-V2	< LoQ (9.4 \cdot 10 ⁻³ \pm 0.6 \cdot 10 ⁻³ mg/mL)

1117

1118

1119

1120 **Table 4.** Overview of interaction energies obtained through the 200 ps sampling at 298 K
1121 (second cycle) simulations in samples with 5% w/w API versus the interaction between
1122 the DeA and DoA in the pure HDES (without API) shown in the first row (n=4, mean \pm
1123 SD).

Molecular interaction energies, kJ/mol				
Interaction type	Hydrogen bonding	Hydrophobic	Pi-Pi	Cation-pi
DeA with DoA (without API)	7179.1 \pm 283.9	9454.0 \pm 79.3	-	-
DeA with DoA (with 5% w/w API)	6195.0 \pm 514.1	9021.7 \pm 330.6	-	-
DeA with API	549.7 \pm 50.4	811.7 \pm 73.4	-	-
DoA with API	263.9 \pm 24.0	430.6 \pm 40.0	-	-

API with API	117.2 ± 16.7	326.4 ± 24.1	52.9 ± 9.1	24.9 ± 6.4
--------------	--------------	--------------	------------	------------

1124

1125

1126

1127 **Table 5.** Overview of venetoclax solubilities (mg/mL) in HDES and with added 10, 20,
1128 and 30% w/w Tween 80 at 25°C after 24, 48 and 72 h and 37°C after 24 h (n=3, mean ±
1129 SD).

Venetoclax solubility (mg/mL) in the LBF mixtures				
Formulation	25°C	25°C	25°C	37°C
	24 h	48 h	72 h	24 h
HDES	100.6 ± 3.2	118.7 ± 0.7	118.2 ± 4.3	118.9 ± 2.0
HDES + 10% w/w Tween 80	104.1 ± 8.2	107.6 ± 2.5	103.9 ± 9.2	111.6 ± 1.0
HDES + 20% w/w Tween 80	109.0 ± 7.2	110.0 ± 4.3	111.3 ± 9.5	105.9 ± 1.7
HDES + 30% w/w Tween 80	102.5 ± 6.6	98.6 ± 1.2	89.8 ± 4.8	57.1 ± 1.7

1130

1131

1132 **Table 6.** Change in droplet diameter in the formulations with and without API (n=3, mean
1133 ± SD).

Formulation	Droplet diameter, µm	
	without API	with 70 mg/mL API

HDES	78.3 ± 24.7	45.5 ± 33.5
HDES + 10% w/w Tween 80	12.4 ± 5.6	44.1 ± 29.8
HDES + 20% w/w Tween 80	7.4 ± 1.7	48.2 ± 28.7
HDES + 30% w/w Tween 80	9.5 ± 4.1	33.9 ± 17.5

1134

1135

1136 **Table 7.** Overview of freezing points of the HDES with 10, 20, 30% surfactant, with and
 1137 without 70 mg/mL of venetoclax (n=3, mean ± SD).

Formulation	Freezing point, °C	
	without API	with 70 mg/mL API
HDES	17.3 ± 0.1	16.8 ± 0.4
HDES + 10 % w/w Tween 80	18.0 ± 0.1	16.0 ± 0.6
HDES + 20 % w/w Tween 80	17.2 ± 0.4	15.0 ± 0.4
HDES + 30 % w/w Tween 80	15.4 ± 0.7	13.7 ± 0.4

1138

1139

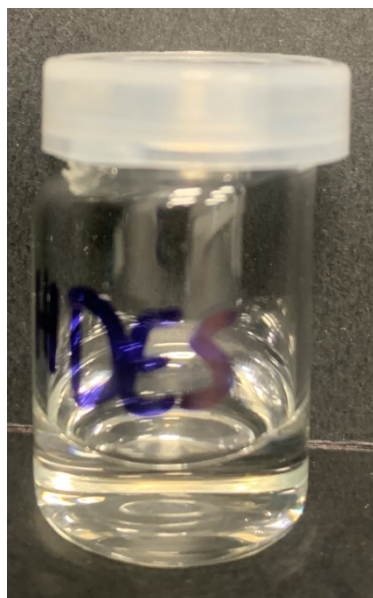
1140 **Table 8.** Overview of dissolved concentration of venetoclax recorded at 120 min (n=3,
 1141 mean ± SD).

Formulation	Concentration of dissolved API, µg/mL
-------------	---------------------------------------

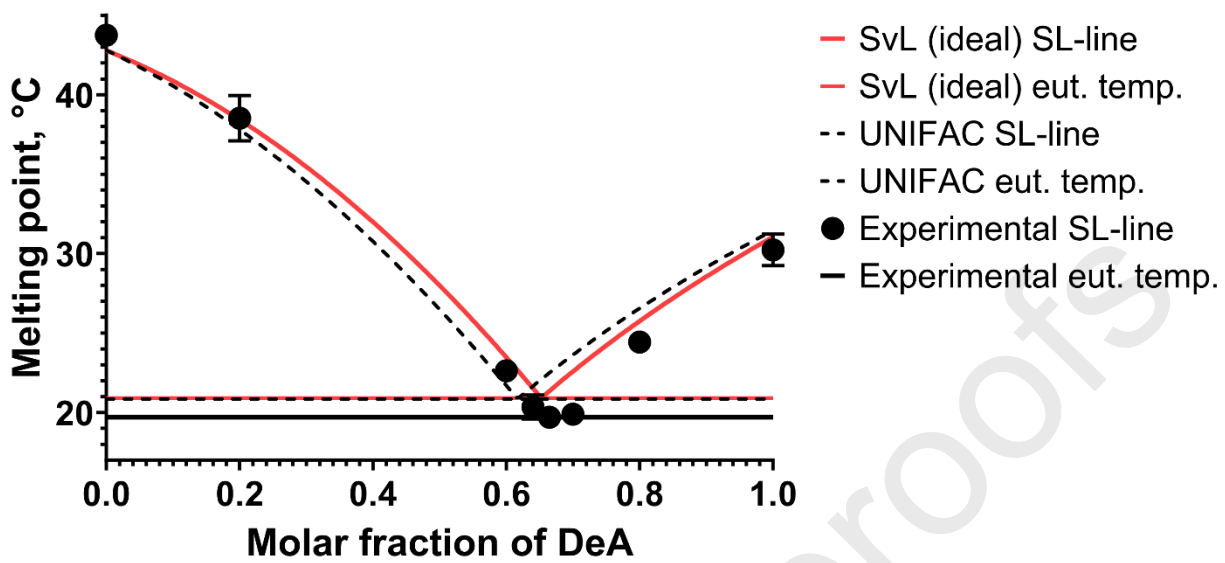
HDES	11.3 ± 1.5
HDES+10% w/w Tween 80	17.5 ± 2.2
HDES+20% w/w Tween 80	27.5 ± 1.4
HDES+30% w/w Tween 80	32.0 ± 0.8

1142

1143



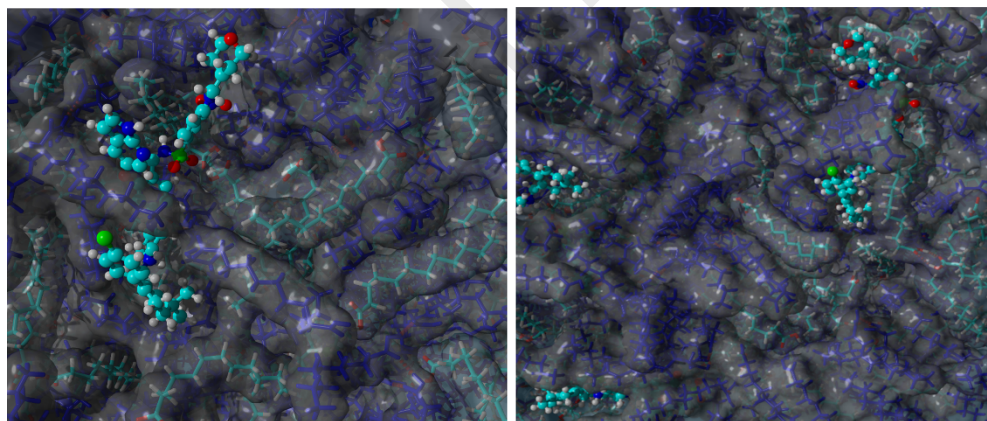
1144



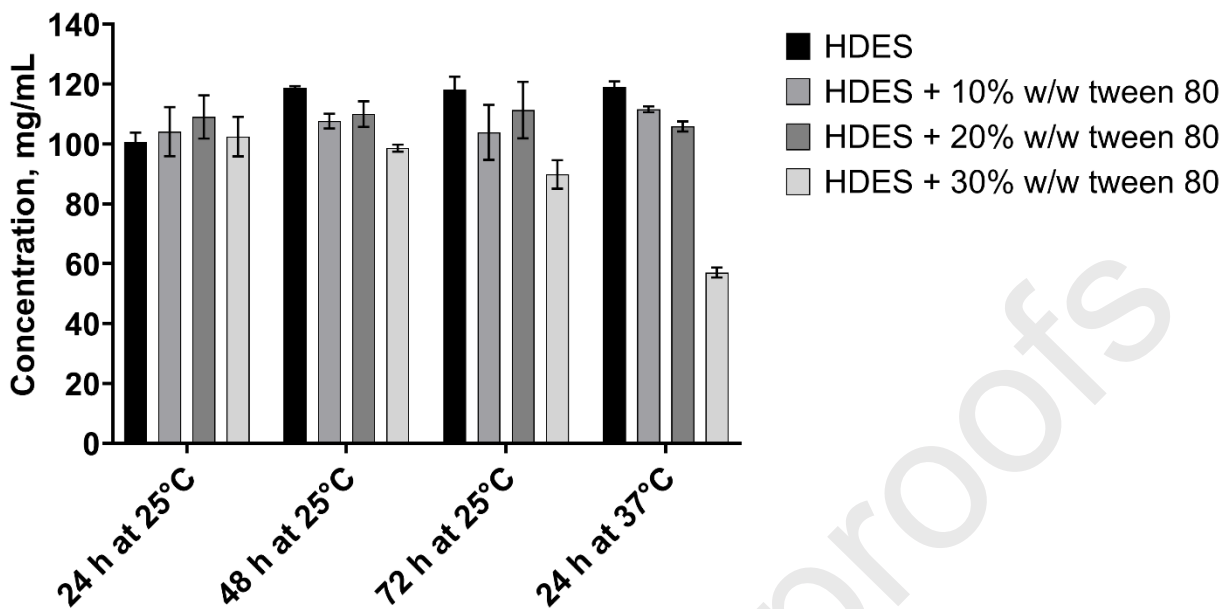
1145



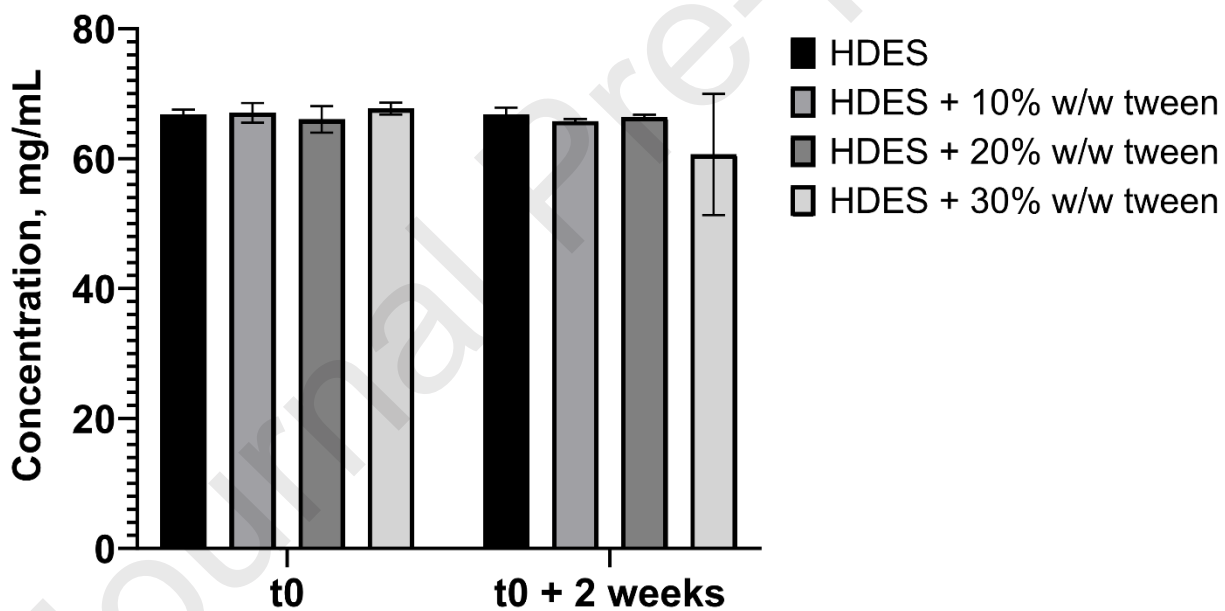
1146



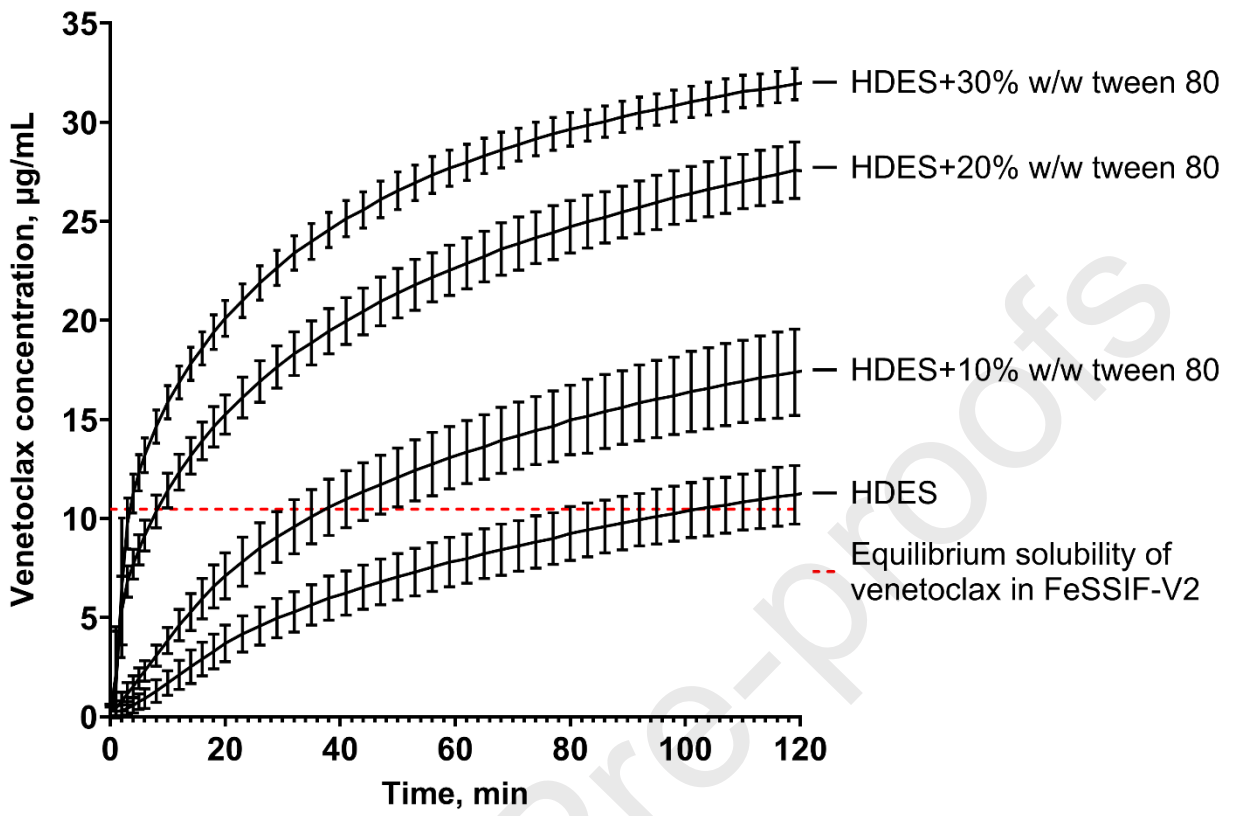
1147



1148



1149



1150